

2023-08-14

# Basolateral amygdala oscillations enable fear learning in a biophysical model

---

M. McCarthy, A. Cattani, N. Kopell, D. Arnold. "Basolateral amygdala oscillations enable fear learning in a biophysical model" eLife.

<https://hdl.handle.net/2144/48635>

*"Downloaded from OpenBU. Boston University's institutional repository."*

# Basolateral amygdala oscillations enable fear learning in a biophysical model

## Reviewed Preprint

Published from the original preprint after peer review and assessment by eLife.

## About eLife's process

## Reviewed preprint posted


August 14, 2023 (this version)

## Sent for peer review

June 14, 2023

## Posted to bioRxiv

May 22, 2023

Anna Cattani , Don B Arnold, Michelle McCarthy, Nancy Kopell

Department of Mathematics & Statistics, Boston University, Boston, Massachusetts, United States • Department of Biology, University of Southern California, Los Angeles, California, United States

 [https://en.wikipedia.org/wiki/Open\\_access](https://en.wikipedia.org/wiki/Open_access)

 <https://creativecommons.org/licenses/by/4.0/>


## Abstract

The basolateral amygdala (BLA) is a key site where fear learning takes place through synaptic plasticity. Rodent research shows prominent low theta (~3-6 Hz), high theta (~6-12 Hz), and gamma (>30 Hz) rhythms in the BLA local field potential recordings. However, it is not understood what role these rhythms play in supporting the plasticity. Here, we create a biophysically detailed model of the BLA circuit to show that several classes of interneurons (PV+, SOM+, and VIP+) in the BLA can be critically involved in producing the rhythms; these rhythms promote the formation of a dedicated fear circuit shaped through rhythmic gating of spike-timing-dependent plasticity. Each class of interneurons is necessary for the plasticity. We find that the low theta rhythm is a biomarker of successful fear conditioning. Finally, we discuss how the peptide released by the VIP+ cell may alter the dynamics of plasticity to support the necessary fine timing.

### eLife assessment

This **useful** modeling study explores how the biophysical properties of interneuron subtypes in the basolateral amygdala enable them to produce nested oscillations whose interactions facilitate functions such as spike-timing-dependent plasticity. The strength of evidence is currently viewed as **incomplete** because the relevance to plasticity induced by fear conditioning is viewed as insufficiently grounded in existing training protocols and prior experimental results, and alternative explanations are not sufficiently considered. This work will be of interest to investigators studying circuit mechanisms of fear conditioning as well as rhythms in the basolateral amygdala.

## Introduction

Pavlovian fear conditioning is widely used as a model of associative learning across multiple species (Phelps and LeDoux, 2005 ) and has been used more generally to study plasticity and memory formation. The major questions, still under investigation, relate to how plasticity is instantiated in defined circuits and how it is regulated by the circuit components (Rumpel et al.,

2005 [↗](#); Sah et al., 2008 [↗](#); Johansen et al., 2014 [↗](#); Bocchio et al., 2017 [↗](#); Grewe et al., 2017 [↗](#)). The fear conditioning paradigm consists of a neutral stimulus (conditioned stimulus, CS) presented one or more times together with an aversive stimulus (unconditioned stimulus, US), which induces a fear response.

In the basolateral amygdala (BLA), the main site of fear learning in the mammalian brain (Fanselow and LeDoux, 1999 [↗](#); Tovote et al., 2015 [↗](#); Krabbe et al., 2018 [↗](#)), local field potential recordings (LFP) show prominent low theta (~3-6 Hz), high theta (~6-12 Hz), and gamma (>30 Hz) rhythms (Seidenbecher et al., 2003 [↗](#); Courtin et al., 2014b [↗](#); Stujenske et al., 2014 [↗](#); Davis et al., 2017 [↗](#)). Recent rodent studies show increased low theta (Davis et al., 2017 [↗](#)) and gamma (Courtin et al., 2014b [↗](#)) in local field potential (LFP) recordings after successful fear conditioning, whereas modulation of high theta is associated with fear extinction (Davis et al., 2017 [↗](#)), a paradigm that aims to suppress the association between CS and fear (Bouton, 2004 [↗](#)); the modulation of the power of these rhythms suggests they may be associated with BLA plasticity.

The origin of the rhythms and their potential roles in instantiating the plasticity needed for successful learning is still under investigation (Bocchio et al., 2017 [↗](#)). Fear responses are mediated by a network of several brain areas including, but not limited to, the BLA, the prefrontal cortex (mPFC), and the hippocampus (Seidenbecher et al., 2003 [↗](#); Stujenske et al., 2014 [↗](#); Tovote et al., 2015 [↗](#)). In experimental studies, successful fear conditioning leads fear-encoding neurons to respond to the CS. In our work, it results in strengthening the connection between neurons encoding CS and neurons encoding fear. We create a biophysically detailed model of the BLA circuit suggesting that interneurons in the BLA can be critically involved in producing the experimentally measured rhythms and are mechanistically important in the instantiation of plasticity during learning. Indeed, we find that the low theta, fast theta, and gamma rhythms in the BLA originating from the BLA interneurons promote the formation of a dedicated fear circuit shaped through rhythmic regulation of depression-dominated spike-timing-dependent plasticity (STDP). (See Discussion about non-depression-dominated plasticity related to fear conditioning.) In this model, if any of the classes of interneurons are removed from the circuit, the rhythms are changed and there is a failure of the plasticity needed for successful learning. We show that fine timing between excitatory projection neurons responding to the CS and US is necessary but not sufficient to produce associative plasticity when the latter can be affected by all the spikes, not just nearest neighbors. The other critical element for plasticity is the interaction of interneurons that creates pauses in excitatory cell activity.

The model reproduces the increase in the low theta after training that was found in the experimental data. This increase was not seen for network instantiations that did not learn; thus, the simulations suggest that the increase in low theta is a biomarker of successful fear conditioning. Furthermore, this low theta signal emanates from the newly formed synapse linking CS- and fear-encoding neurons. These results are also highly relevant to the recent study (Perrenoud and Cardin, 2023 [↗](#); Veit et al., 2023 [↗](#)) in which the same types of interneurons used in this paper are shown to allow global selectivity in coherence in gamma oscillations (see Discussion).

## Results

### Rhythms in the BLA can be produced by interneurons

Brain rhythms are thought to be encoded and propagated largely by interneurons (Whittington et al., 2000 [↗](#)). Identified interneurons in BLA include VIP (vasoactive intestinal peptide-expressing), SOM (somatostatin-expressing), and PV (parvalbumin-expressing) (Muller et al., 2006 [↗](#), 2007 [↗](#); Rainnie et al., 2006 [↗](#); Bienvu et al., 2012 [↗](#); Krabbe et al., 2018 [↗](#), 2019 [↗](#)), which can be further

subdivided according to their electrophysiological dynamics (Sosulina et al., 2010; Spampanato et al., 2011). In the model, we show that some types of VIP, SOM, and PV can each contribute to the generation of a key rhythm involved in the BLA due to their specific intrinsic currents.

For VIP interneurons, we consider a subtype that responds to a depolarizing step current with bursting or stuttering behavior (Sosulina et al., 2010; Spampanato et al., 2011). This type of behavior can be elicited by a D-type potassium current, a current thought to be found in a similar electrophysiological subtype of VIP interneurons in the cortex (Porter et al., 1998). In our model, VIP interneurons endowed with a D-current respond to depolarizing currents with long bursts, and to hyperpolarizing currents with no action potentials, thus reproducing the electrophysiological properties of type I BLA interneurons in (Sosulina et al., 2010) (Fig. 1A, top): our VIP neurons exhibit gamma (~52 Hz) bursting activity at low theta frequencies (~3-6 Hz) in the baseline condition, the condition without any external input from the fear conditioning paradigm (Fig. 1B, top).

SOM interneurons have been well studied in the hippocampus, especially the O-LM cells (Maccaferri and McBain, 1996; Gillies et al., 2002; Saraga et al., 2003; Rotstein et al., 2005). Although the intrinsic currents of BLA SOM cells are unknown, SOM cells in the hippocampus have a hyperpolarization-activated current, i.e., H-current, and a persistent sodium current, i.e., NaP-current. In our model, with the introduction of these currents with specific conductances (see Materials and Methods for details), the SOM cells mimic the electrophysiologic behavior of type III BLA SOM cells in (Sosulina et al., 2010), showing regular spikes with early spike-frequency adaptation in response to a depolarizing current, and pronounced inward rectification (downward deflection) and outward rectification (upward deflection) upon the initiation and release of a hyperpolarizing current (Fig. 1A, middle). In our baseline model, SOM cells have a natural frequency rhythm in the high theta range (6-12 Hz) (Fig. 1B, middle).

Our model PV interneurons are fast-spiking interneurons (FSIs) with standard action potentials produced by Hodgkin-Huxley-type sodium and potassium conductances. They are silent at baseline condition and show similar behaviors to type IV interneurons (Sosulina et al., 2010) in response to depolarizing and hyperpolarizing currents (Fig. 1A, bottom). At baseline, our PV interneurons are silent (Fig. 1B, bottom). However, when reciprocal connections are present and the excitatory projection neuron receives enough excitation to fire, the PV interneuron forms a PING rhythm (pyramidal-interneuron network gamma) (Whittington et al., 2000) (Fig. 1C); this has been suggested as a possible mechanism for the basis of gamma rhythm generation in the BLA (Feng et al., 2019). The reciprocal interactions between the projection neuron and PV form a gamma rhythm that depends sensitively on the external input to the excitatory projection neuron and the PV's decay time constant of inhibition (8.3 ms).

## Interneurons interact to modulate fear neuron output

Our BLA network consists of interneurons, detailed in the previous section, and excitatory projection neurons (Fig. 2A). In response to the noxious stimulus US, this network produces all the rhythms originating from the interneurons, as shown in Fig. 1. The simplest network we consider is made of one neuron for each cell type. We introduce some heterogeneity in the last two sections of the Results.

Both the fear-encoding neuron (F), an excitatory projection neuron, and the VIP interneuron are activated by the noxious stimulus US (Krabbe et al., 2019). As shown in Fig. 2A (top, right), VIP disinhibits F by inhibiting both SOM and PV, as suggested in (Krabbe et al., 2019). Since VIP is active during both rest and upon the injection of US, it then modulates F at low theta cycles via SOM and PV. We do not include connections from PV to SOM and VIP, nor connections from SOM to PV and VIP, since those connections have been shown to be significantly weaker than the ones included (Krabbe et al., 2019). Fig. 2A (bottom) shows a typical dynamic of the network before and after the US input onset. In the baseline condition, the VIP interneuron has short

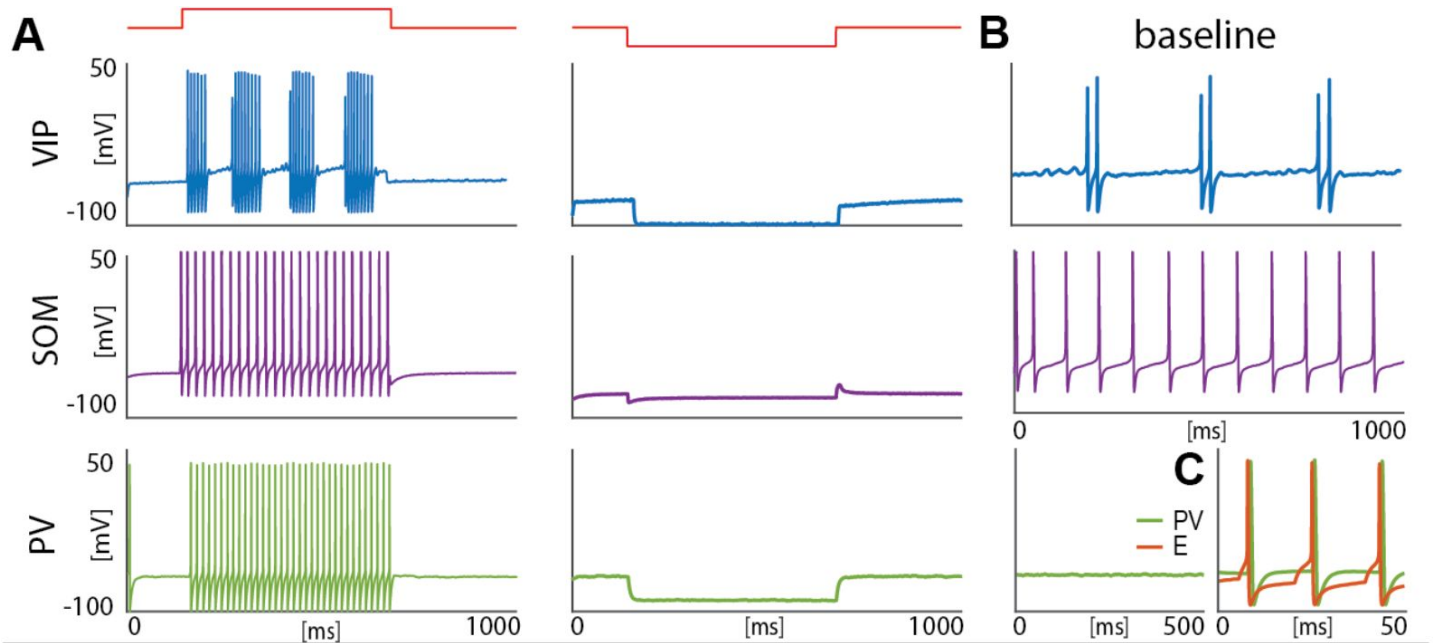


**Figure 1.**

**Isolated neurons produce fundamental rhythms.**

**A.** dynamics in response to depolarizing and hyperpolarizing currents mimic the electrophysiological behavior of BLA interneurons classified in (Sosulina et al., 2010). **B.** dynamics in the baseline condition. **C.** Interacting PV and excitatory projection neuron (E) entrain in a pyramidal-interneuron network gamma rhythm (PING).

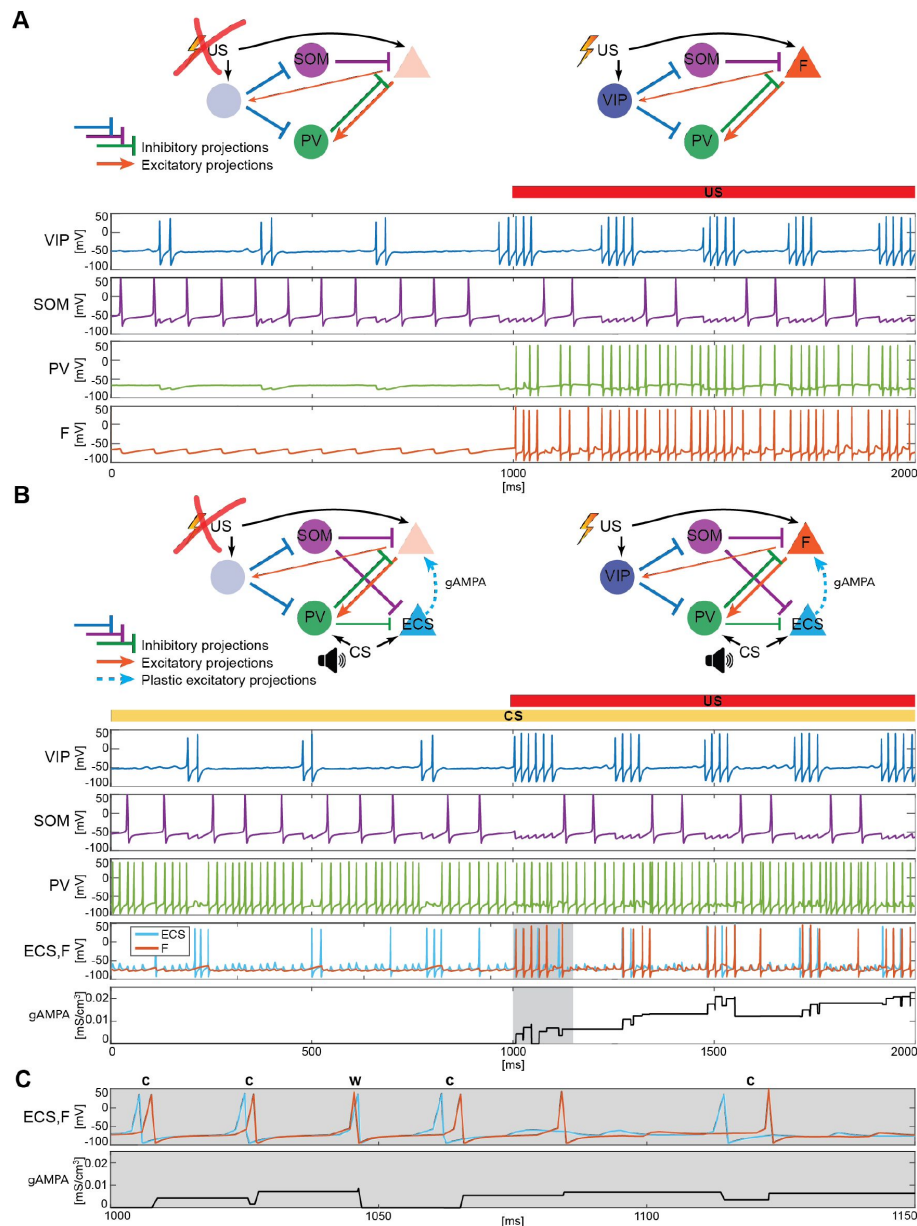


**Figure 2.**

**BLA interneurons and the excitatory projection neurons interact and modulate the network activity.**

**A (top):** Network made of three interneurons (VIP, SOM, and PV) and the excitatory projection neuron encoding fear (F) without US input (left) and with US input (right). **A (bottom):** before the onset of US, VIP shows gamma bursts nested in the low theta rhythm (blue trace), and SOM fires at a natural frequency in the high theta range (purple trace). PV is completely silent due to the lack of any external input (green trace). F, despite its natural frequency of around 11 Hz, is silent due to the inhibition from SOM (orange trace). After US onset, due to the longer VIP bursts and the US input, F shows a pronounced activity during the VIP active phase and outside when the SOM and PV inhibition fade. PV is active only when excited by F, and then gives inhibitory feedback to F. **B (top):** Network in panel A with the excitatory projection neuron encoding the CS input (ECS) during the CS presentation (left) and with paired CS and US inputs (right). **B (bottom):** 2-second dynamics of all the neurons in the BLA network affected by CS, and by US after 1 second has elapsed. As in panel A, VIP shows gamma bursting activity nested in the low theta frequency range with bursts duration affected by the presence or absence of US. VIP inhibits i) SOM, which fires at high theta (purple trace) regardless of the external inputs, and ii) PV, which fires at gamma. ECS (light blue trace) and F are both active when both CS and US are present and VIP is active, producing a gamma nested into a low theta rhythm. The evolution in time of the conductance (gAMPA) shows an overall potentiation over the second half of the dynamics when both ECS and F are active. **C:** blowup of ECS-F burst of activity and gAMPA dynamic shown in the gray area in panel B (bottom); ECS (blue trace) fires most of the time right before F, thus creating the correct pre-post timing conducive for potentiation of the ECS to F conductance. The order of each pair of ECS-F spikes is labeled with “c” (correct) or “w” (wrong).

gamma bursts nested in low theta rhythm. With US onset, VIP increases its burst duration and the frequency of low theta rhythm. These longer bursts make the SOM cell silent for long periods of each low theta cycle, providing F with windows of disinhibition and contributing to the abrupt increase in activity right after the US onset. Finally, in [Fig. 2A](#), PV lacks any external input and fires only when excited by F. Thanks to their reciprocal interactions, PV forms a PING rhythm with F, as depicted in [Fig.1C](#).

## Interneuron rhythms provide the fine timing needed for depression-dominated STDP to make the association between CS and fear

We now introduce another excitatory projection neuron (ECS), as shown in [Fig. 2B](#) (top). ECS, unlike F, responds to the neutral stimulus CS, as does PV. By the end of fear conditioning, CS consistently activates the neuron F, thus eliciting the network fear response. This happens because of the formation and strengthening of the synapse from ECS to F by means of synaptic plasticity. We now show how this network, with appropriate connection strengths among neurons, can make the timing of the interneurons confer pre-post timing to ECS and F, which is conducive to spike-timing-dependent plasticity potentiation suggested to be critical for associative aversive learning ([Rogan et al., 1997](#); [Nabavi et al., 2014](#)); in particular, we need feedback inhibition (from PV to F) to be stronger than lateral inhibition (from PV to ECS) to promote ECS firing before F. The Hebbian plasticity rule that we use is characterized by a longer time constant of depression than potentiation (and equal maximal amplitudes) and considers the whole history of ECS and F spiking activity (see Materials and Methods and [Fig. S1A](#) for more details).

[Fig. 2B](#) (bottom) shows an example of the network dynamics with CS present for 2 seconds and US injected after the first second of simulation. ECS is active during the whole 2-second interval. CS also affects PV, which is active most of the time; F is active only in the second half of the dynamics when US is also present. All the rhythms generated by the interneurons are apparent in response to CS and simultaneous CS-US inputs, and they are generated by the same mechanisms as in the fear-only network ([Fig. 2A](#)). In contrast to the fear-only network, the projection neurons F and ECS are both modulated by the VIP low theta rhythm. This is because the PV increased activity due to CS tends to silence (with the help of SOM) ECS and F during the silent VIP phase at low theta. During the active VIP phase, however, both ECS and F are active, and the simulations show that ECS fires most of the time slightly before F (see [Fig. 2B,C](#) and [Fig. S1B](#)); this fine timing needed for potentiation is established by the PING rhythm (see [Fig. 1C](#)). By contrast, in the first second of the simulation in [Fig. 2B](#) (bottom), SOM and PV prevent plasticity by silencing F, which in the absence of US receives only a weak applied current: thus, without concurrent US and CS, STDP cannot occur between ECS and F. In the next sections, we will explore the role of each interneuron and its associated rhythm in shaping the network dynamics and allowing the association between CS and fear to be instantiated.

## With the depression-dominated plasticity rule, all interneuron types are needed to provide potentiation during fear learning

We now show that, in the example used above, only the network endowed with all the interneurons and their associated rhythms leads to overall potentiation of the conductance from ECS to F in the timeframe used to induce the fear learning in experimental work. (see Discussion for other plasticity rules.) In general, experimental work finds successful learning after one or very few presentations of CS and US (lasting 1.5 or 2 seconds) interspersed with CS-only intervals lasting 30-40 seconds (e.g., see ([Davis et al., 2017](#); [Krabbe et al., 2019](#))). The 40-second interval we consider consists of US and CS active during the entire period: since an initial bout of US is known to produce a long-lasting fear response beyond the offset of the US ([Hole and Lorenz, 1975](#)), we treat the US as present (e.g., for 1.5 or 2 seconds) followed by US activity induced by memory for the remainder of the 40 seconds.

**Fig. 3A** shows the evolution of the average ECS to F AMPA maximal conductance during fear conditioning across 40 network realizations of the full network, as well as from networks lacking VIP, PV, SOM. The average ECS to F AMPA conductance robustly potentiates only in the network containing all three interneurons (**Fig. 3A**; see Fig. S3 for exceptions outside the normal physiological range). Furthermore, as shown in **Fig. 3B**, all the full network realizations are “learners”. We define *learners* as those realizations whose AMPA conductance from ECS to F is higher than  $0.12 \text{ mS/cm}^3$  at the end of the 40-second interval, which results in the systematic activation of the fear neuron F following each ECS spike when only CS is presented. This is consistent with the high rate of successful learning in rodent experiments after one pairing of CS and US, despite inter-individual differences among animals (Schafe et al., 2000). Network realizations differ from one another in the initial state of each neuron involved, and all receive independent Gaussian noise.

We show in **Fig. 3C** results in which we relax the assumption that US is active over the entire forty seconds by allowing US to be active only during the initial 15 seconds of the fear conditioning paradigm. We find that learning may still occur under this condition. The reason is that, after 15 seconds of CS and US pairing, ECS to F may have potentiated enough that ECS can drive F some of the time (although not all the time). This allows further potentiation to occur in the presence of CS alone. We find that, if the conductance from ECS to F is higher than a threshold value of  $0.037 \text{ mS/cm}^3$  after the 15 seconds of CS and US presentation, then the network will become a learner after a further thirty seconds of CS alone; those network realizations that did not reach the threshold value are defined here as *non-learners*. Even with this more realistic assumption, the large majority of network realizations were learners (19 out of 20 networks). This is in agreement with the experimental fear conditioning literature showing that most of the subjects learn the association between CS and fear after only one trial (Schafe et al., 2000).

## Physiology of interneuron types is critical to their role in appropriate plasticity

The PV cell is necessary to induce the correct pre-post timing between ECS and F needed for long-term potentiation of the ECS to F conductance. In our model, PV has reciprocal connections with F and provides lateral inhibition to ECS. Since the lateral inhibition is weaker than the feedback inhibition, PV tends to bias ECS to fire before F. This creates the fine timing needed for the depression-dominated rule to instantiate plasticity. If we used the classical Hebbian plasticity rule (Bi and Poo, 2001) with gamma frequency inputs, this fine timing would not be needed and ECS to F would potentiate over most of the gamma cycle, and thus we would expect random timing to lead to potentiation (Fig. S2). In this case, no interneurons are needed (See Discussion).

In this network configuration, the pre-post timing for ECS and F is repeated robustly over time due to coordinated gamma oscillations (PING, as shown in **Fig. 4A**, **Fig. 1C**, and **Fig. 2B,C**) arising through the reciprocal interactions between F and PV (Feng et al., 2019). PING can arise only when PV is in a sufficiently low excitation regime such that F can control PV activity (Börgers et al., 2005), as in **Fig. 4A**. However, despite PING establishing the correct spike-timing for potentiation, setting PV in a low excitation regime in which F-PV PING occurs continuously does not lead to potentiation (**Fig. 4A**, Fig. S1C): the depression-dominated rule leads to depression rather than potentiation unless the PING is periodically interrupted. During the pauses, made possible only in the full network by the presence of VIP and SOM, the history-dependent build-up of depression decays back to baseline, allowing potentiation to occur on the next ECS/F active phase. (The detailed mechanism of how this happens is in the Supplementary Information, including Fig. S1). Thus, a network without the other interneuron types cannot lead to potentiation.

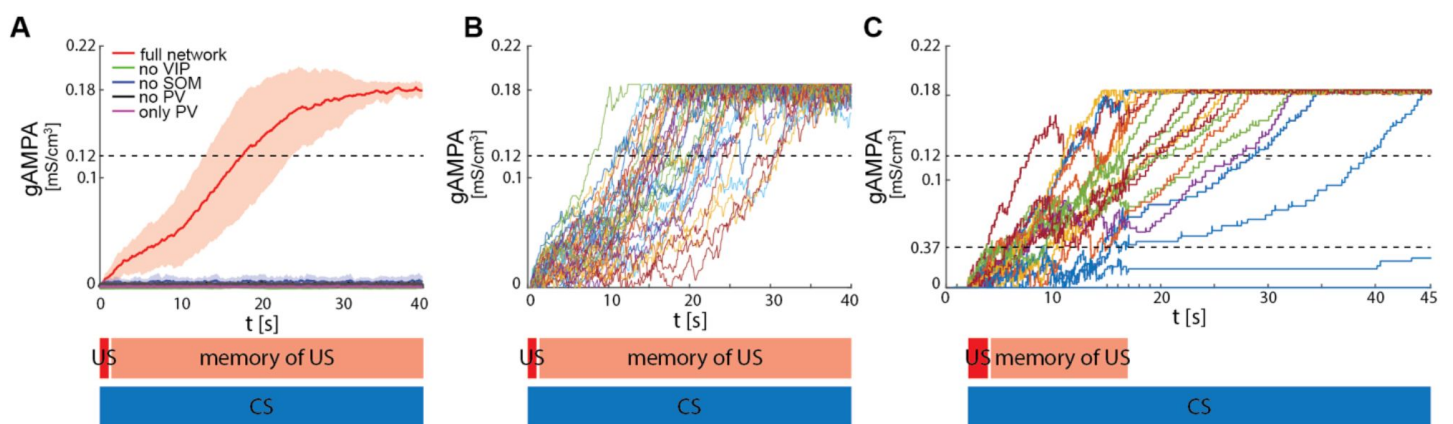


**Figure 3.**

### ECS to F conductance across network realizations.

**A:** Mean (color-coded curves) and standard deviation (color-coded shaded areas) of the AMPA conductance (gAMPA) from ECS to F across 40 network realizations over 40 seconds. Red curve and shaded area represent the mean and standard deviation, respectively, across network realizations endowed with all the interneurons. **B:** Evolution in time of the AMPA conductance for the 40 full network realizations in A. **C:** AMPA conductance of 20 network realizations over 45 seconds with F strongly activated by US (2 seconds) and its memory (13 seconds), and ECS active the whole interval because of CS; 19 out of 20 network realizations show potentiation after one trial.

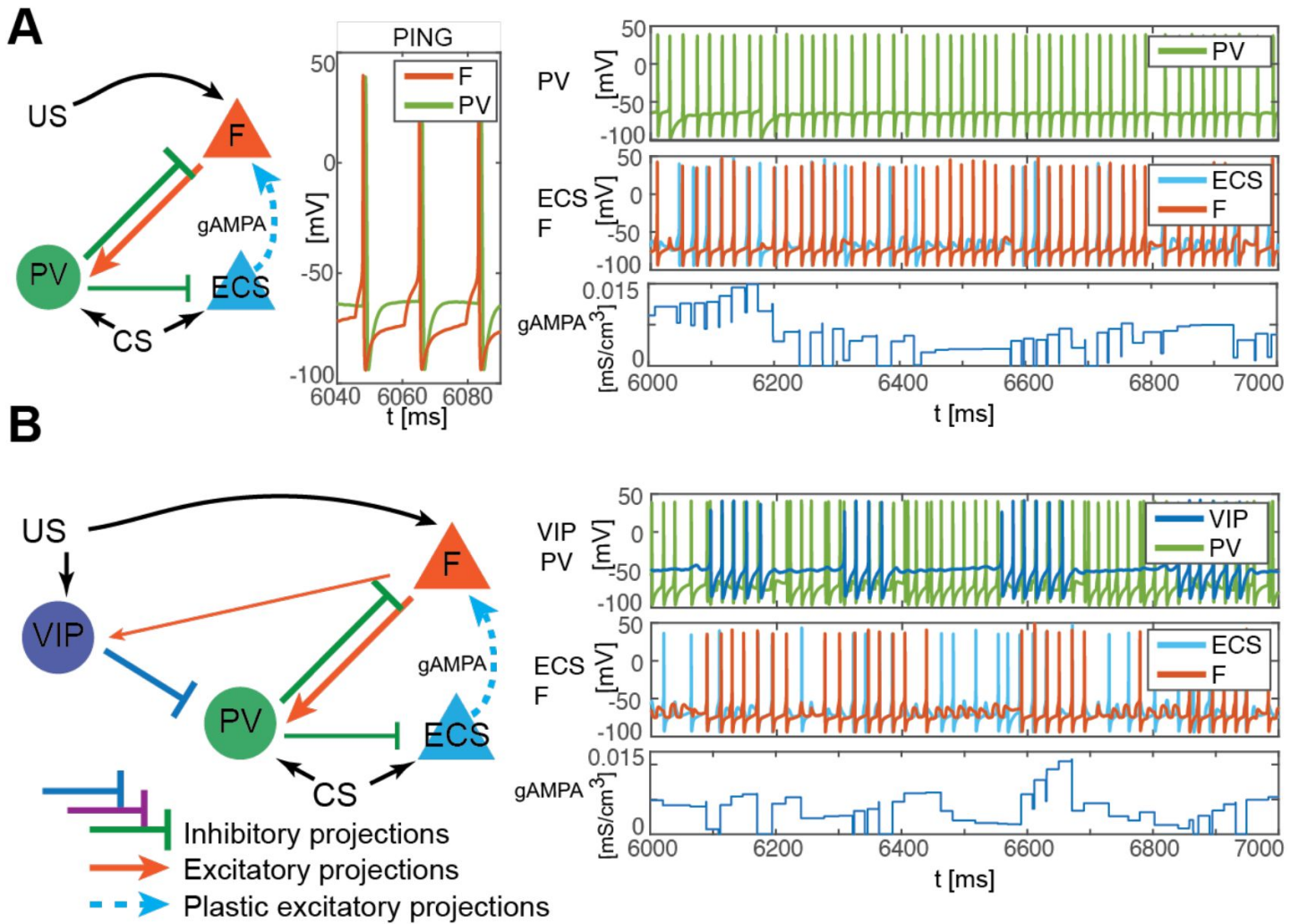


**Figure 4.**

**PV-only network and VIP-PV network lead to depression.**

**A:** Left, network with PV as the only interneuron. PV cell is at an excitation level that supports PING. Middle, dynamics of PV and F that reciprocally interact and generate PING. Right, PV and F entrain in PING (top), ECS and F activity (middle), and evolution in time of the ECS to F AMPA conductance (bottom). **B:** Left, network with both PV and VIP. Right, network dynamics (top, middle) followed by the evolution in time of the ECS to F AMPA conductance (bottom). The detailed mechanism behind the evolution of AMPA conductance in panels A and B is in the Supplementary Information, including Fig. S1.

In our simulations (except for the one in [Fig. 4A](#)), we choose to set PV cells at a high excitation level due to a strong input from CS in order to account for: (i) the experimental literature showing a strong activation of PV after the onset of CS ([Wolff et al., 2014](#)); (ii) many other inputs that the PV cell receive besides CS. We show in [Fig. S3A](#) that increasing the PV excitation by adding other inputs to PV cells leads to similar results; all interneurons are necessary for ECS to F potentiation under these circumstances. If CS activation of PV is weakened, we find potentiation can occur in the absence of VIP and SOM ([Fig. S3B](#)). However, we consider this outside the physiological range.

In the context of high PV excitation, we find that the VIP cell plays two critical roles in enabling potentiation to occur via PING. First, it reduces the excitation of the PV cell during its active low-theta phase, enabling the PV cell to participate in PING ([Fig. 4B](#), [Fig. S1D](#)). Second, it provides the periodic interruptions in ECS and F firing necessary for potentiation during its silent low-theta phase. Without these pauses, depression dominates (see SI section “ECS and F activity patterns determine overall potentiation or depression”). This interruption requires the participation of another interneuron, the SOM cell ([Figs. 2B](#), [4B](#), [S1](#)): the pauses in inhibition from the VIP periodically interrupt ECS and F firing by releasing PV and SOM from inhibition and thus indirectly silencing ECS and F.

## Network with multiple heterogeneous neurons can establish the association between CS and fear

To test the robustness of our single-cell results to heterogeneity, we expand our BLA network to include three cells of each interneuron subtype and ten of each excitatory projection neuron ([Fig. 5A](#)). Each neuron has independent noise and cellular parameters (see Materials and Methods for details). We find that the network very robustly produces potentiation between the ECS and F receiving CS and US, respectively, during fear training, with additional properties matching the experimental results.

[Fig. 5B](#) shows an example of the network dynamics during fear conditioning with simultaneous CS and US inputs. As previously presented for the single neuron network ([Figs. 2-3](#)), interneurons are crucial in conferring the correct pre-post spike timing to ECS and F. We assume all the VIP interneurons receive the same US; hence, the VIP neurons tend to approximately synchronize at low theta in response to US input, allowing a window for potentiation of ECS to F conductance ([Fig. 5B](#)), as we have seen in the single cell model. The potentiation from ECS to F is specifically for the excitatory projection cells receiving CS and US, respectively ([Fig. 5C](#)). The ECS cells not receiving CS are inhibited by ongoing PV activity during the disinhibition window ([Fig. 5B](#)); they are constructed to be firing at 11 Hz in the absence of any connections from other cells. The lack of activity in those cells during fear conditioning implies that there is no plasticity from those ECS cells to F. This larger network corroborates the results obtained for the single neuron network: only the realizations of the full network learn the association between CS and fear ([Fig. 5D](#), left) and all those network realizations become learners in less than forty seconds ([Fig. 5D](#), right). Similarly, there is a striking failure of plasticity if any interneuron is removed from the network; even partial plasticity does not arise.

## Increased low-theta frequency is a biomarker of fear learning

In this section, we explore how plasticity in the fear circuit affects the network dynamics, comparing after fear conditioning to before. We first show that fear conditioning leads to an increase in LFP low theta frequency power compared to pre-conditioned level ([Fig. 6A,B](#)); there is no change in the high theta power. These results reproduce the experimental findings in ([Davis et al., 2017](#)). We find that the newly potentiated AMPA current from ECS to F is the main source of increase in the low theta power ([Fig. 6C](#)). The increase in power is in the low theta range because ECS and F are allowed to spike only during the active phase of the low theta spiking VIP neurons.

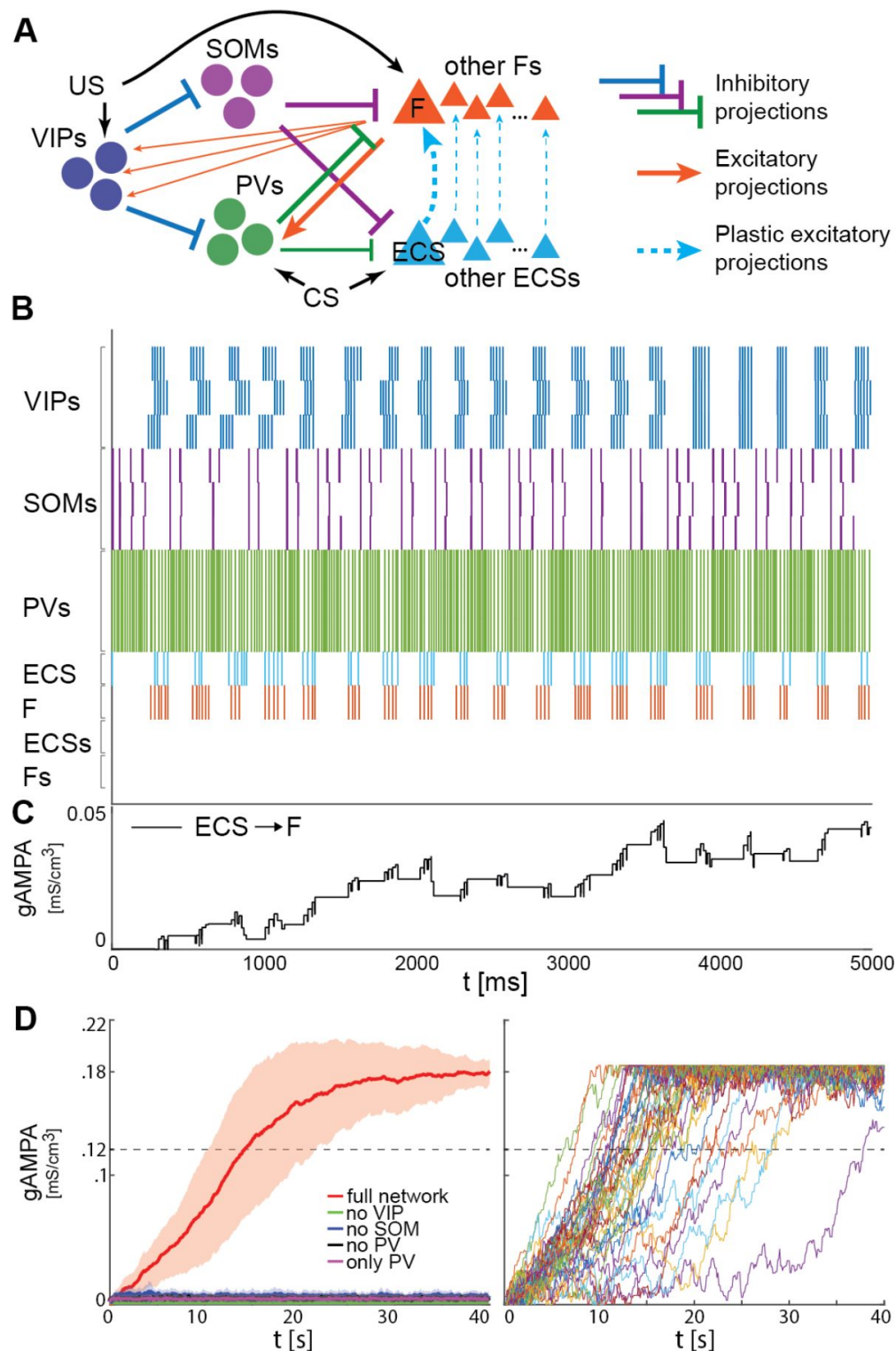


**Figure 5.**

**Heterogeneous BLA fear network is capable of establishing the association between CS and fear.**

**A:** whole BLA network with multiple and heterogeneous neurons. **B:** Dynamics in the first 5000 ms of each of the neurons in the BLA network. **C:** Dynamics of ECS to F conductance over 5000 ms shaped by the activity in **B**. **D:** Left, mean and standard deviation across 40 network realizations of the ECS to F conductance for the full (red), no VIP (green), no SOM (purple), no PV (black), no SOM and PV (magenta) networks. The green, purple, black, and magenta curves are superimposed on each other. Right, dynamics of all the 40 full network realizations over 40 seconds.

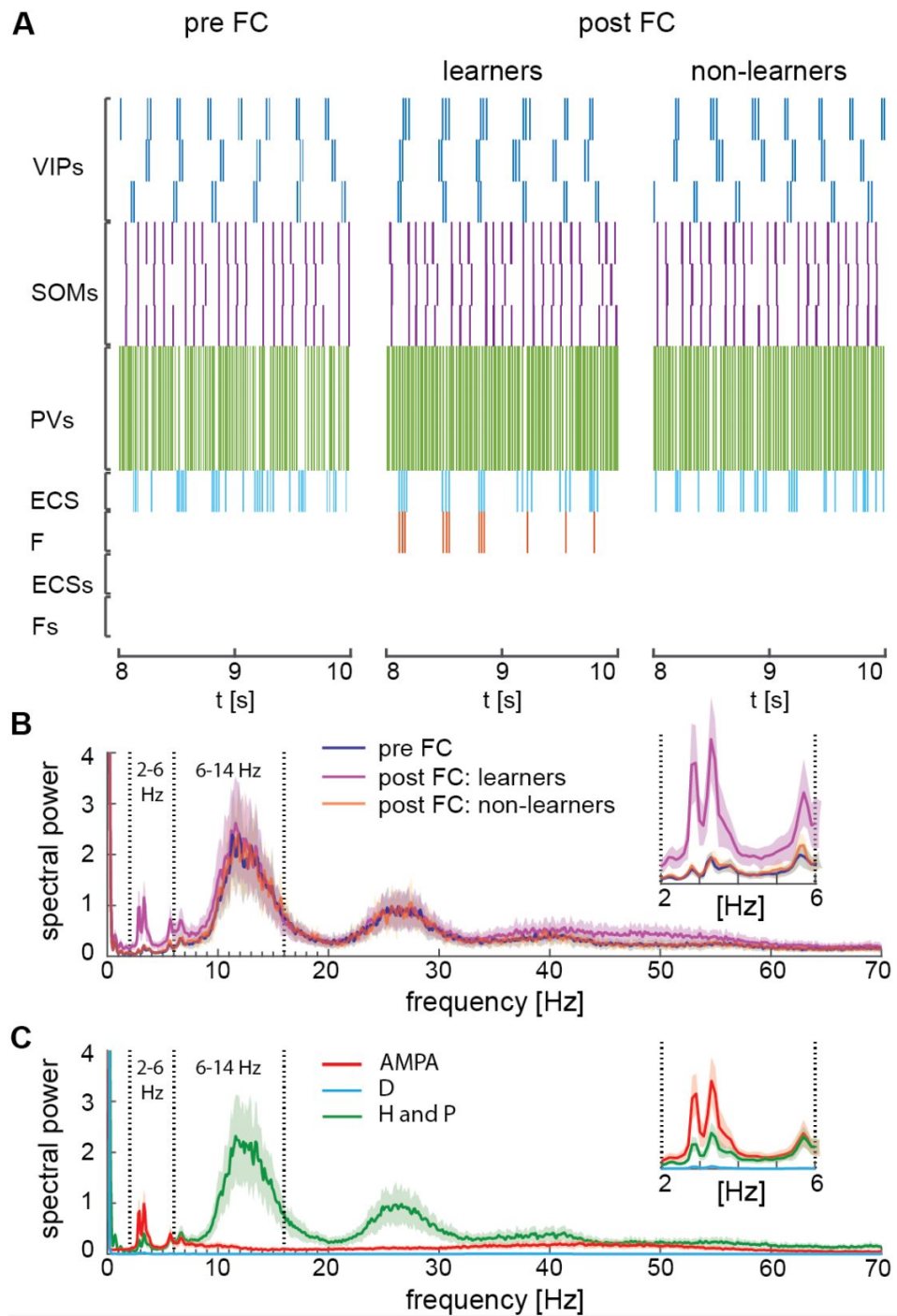


**Figure 6.**

**Heterogeneous network dynamics and spectral properties pre versus post fear conditioning for network realizations in learners and non-learners.**

**A:** Dynamic of BLA heterogeneous networks pre (left) and post (learner, middle; non-learner, right) fear conditioning. **B:** Power spectra mean and standard deviation across 40 network realizations before fear conditioning (blue) and after successful (purple) and non-successful fear conditioning (orange); top, right: inset between 2 and 6 Hz. Blue and orange curves closely overlap. **C:** Power spectra mean and standard deviation across 40 network realizations of LFP signals derived from AMPA currents (red curve), D-current (light blue curve), NaP-current and H-current (green curve); top, right: inset between 2 and 6 Hz. AMPA currents are calculated from the interactions from ECS to F, F to VIP cells, and F to PV. VIP cells contribute to the D-current and SOM cells to H-current and NaP-current (see the result's section "Rhythms in the BLA can be produced by interneurons" for a description of these currents).

Although the experimental results in (Davis et al., 2017) show an increase in low theta after fear learning, they excluded non-learners from their analysis, and thus is unclear from their results if low theta can be used as a biomarker of fear learning. To address this question, we looked at the power spectra after fear conditioning in learning versus non-learning networks. To have an adequate number of non-learners, we ran 60 network simulations for 10 seconds and chose those whose conductance from ECS to F remained lower than  $0.037 \text{ mS/cm}^3$  (i.e., *non-learners*). Notably, the low theta power increase is completely absent after fear conditioning in those network realizations that display no signs of learning. This suggests low theta power change is not just an epiphenomenon but rather a biomarker of successful fear conditioning.

Finally, we find a trend towards increased power in the gamma range between 35 and 60 Hz compared to pre-conditioned level, which supports experimental results in (Courtin et al., 2014b).

## Plasticity between fear neuron and VIP slows down overall potentiation

In-vivo studies documented plastic connections involving GABAergic interneurons in addition to those among excitatory projection neurons (Szinyei et al., 2007; Lucas et al., 2016). VIP interneurons play a crucial role in enabling the association between CS and fear in the fear circuit; hence, we studied the effect that potentiation in the conductance from the fear neuron F to the VIP interneurons, acquired during fear conditioning, has on the potentiation from ECS to F. We find that such a plastic connection in both the single-neuron network and the heterogeneous network can lead to preventing some realizations from learning the association between CS and fear in the first forty seconds; this is because strengthening of the F to VIP connections slow down the potentiation from ECS to F (Fig. S4-S5). Further details on the F to VIP plasticity rule and the role of the F to VIP conductance in slowing down the association between CS and fear can be found in section “Plasticity between fear neuron and VIP slows down overall potentiation” in the Supplementary Information.

We also find that plasticity between the fear neuron and VIP interneurons helps increase even further the low theta power after fear conditioning compared to before (Fig. S6). Further details can be found in section “Plastic F to VIP connections further increase low-theta frequency power after fear conditioning” in the Supplementary Information.

## Discussion

### Overview

Our study suggests that amygdalar rhythms play a crucial role in plasticity during fear conditioning. Prominent rhythms found in the BLA during fear conditioning include low theta (3-6 Hz), high theta (6-12 Hz), and gamma (>30 Hz) (Seidenbecher et al., 2003; Courtin et al., 2014b; Stujenske et al., 2014; Davis et al., 2017). Experimental work in rodents shows that the BLA undergoes more oscillatory firing at low theta frequency and gamma following fear conditioning, while high theta frequency remains unchanged compared to before fear conditioning (Courtin et al., 2014b; Davis et al., 2017).

To examine the origin of these rhythmic changes and their functional role in fear conditioning, we implement a biophysically detailed model of the BLA. We show that vasoactive intestinal peptide-expressing (VIP) interneurons, parvalbumin-expressing (PV) interneurons, and somatostatin-expressing (SOM) interneurons in the BLA may be centrally involved in producing the experimentally measured rhythms based on the biophysical properties of these interneurons. More specifically: the gamma oscillation is associated with PV cell interaction with excitatory cells

to produce PING; VIP cells produce low theta due to their intrinsic D-current; SOM cells help produce the high theta rhythm due to persistent sodium current (NaP-current) and H-currents. Moreover, we show that the rhythmic dynamics produced by VIP and PV cells both play a crucial role in the instantiation of plasticity during associative learning by promoting the formation of a dedicated fear circuit shaped through spike-timing-dependence and the removal of any of the interneuron types from the circuit leads to failure of the plasticity needed for associative fear learning. We note that the presence of SOM cells is crucial for plasticity in our model since they help to produce the necessary pauses in the excitatory projection cell activity. However, the high theta rhythm they produce is not crucial to the plasticity: in our model, high theta or higher frequency rhythms in SOM cells are all conducive to associative fear learning. This opens the possibility that the high theta rhythm in the BLA mostly originates in the prefrontal cortex and/or the hippocampus (Stujenske et al., 2014 [↗](#), 2022 [↗](#)). Finally, we replicate the experimental increase in the low theta after successful training (Davis et al., 2017 [↗](#)) and determine that this is a biomarker of fear learning, i.e., the increase in low-theta power does not appear in the absence of learning.

## Synaptic plasticity in our model

Synaptic plasticity is the mechanism underlying the association between neurons that respond to the neutral stimulus CS (ECS) and those that respond to fear (F), which instantiates the acquisition and expression of fear behavior. One form of experimentally observed long-term synaptic plasticity is spike-timing-dependent plasticity (STDP), which defines the amount of potentiation and depression for each pair of pre- and postsynaptic neuron spikes as a function of their relative timing (Bi and Poo, 2001 [↗](#); Caporale and Dan, 2008 [↗](#)). There are many STDP rules in the literature (Abbott and Nelson, 2000 [↗](#); Feldman, 2012 [↗](#)) but none we are aware of specifically for the amygdala. The depression-dominated Hebbian rule, which we use in this study, provides each interneuron subtype with a specific role in allowing the instantiation of fear learning. With this rule, depression is overall stronger than potentiation, unless there is fine timing among pyramidal cells in the gamma and low theta cycles.

With the depression-dominated rule, each interneuron plays a role in setting up this fine timing in the gamma and low theta cycles needed for appropriate plasticity. PV interneurons are important in creating a gamma rhythm with F when the latter is activated by the unconditioned stimulus (US). This gamma rhythm plays a central role in the fine timing between ECS and F. As mentioned earlier, the critical requirements for plasticity are a pause of VIP firing within each low-theta cycle and fine timing of the ECS (pre) and F (post) neurons in the active phase of the cycle. The pause in VIP cell firing allows for activation of SOM cells, which helps to inhibit the ECS and F cells. Without the pause, the ECS and F cells continue to fire. It is a consequence of the depression-dominated rule that this would lead to depression; this happens because the depression does not relax to zero between gamma-frequency spikes, and hence continues to build up. With a Hebbian plasticity rule characterized by a lower amplitude for depression than for potentiation, potentiation would occur at most of the phases of gamma and thus fine timing would not be needed (Fig. S2). The depression-dominated rule allows for regulation of the plasticity by modulation of all the kinds of cells that are known to be involved in fear learning as well as providing reasons for the known involvement of rhythms. It remains to be understood how lack of such regulation might produce deficits in fear learning.

VIP cells may be important in establishing the kind of depression-dominated rule we are using in this model for the synapse between ECS and F. VIP cells are known to corelease the peptide VIP along with GABA (Bayraktar et al., 1997 [↗](#)). The amount of the release is related to the amount of high frequency firing, i.e., the duty cycle of the gamma burst in each low theta cycle (Agoston et al., 1988 [↗](#); Agoston and Lisiewicz, 1989 [↗](#)). The peptide VIP can act on second messenger pathways to inhibit potentiation; the pathways are complex and not fully understood, but in hippocampus they involve GABA transmission, NMDA activation, and CaMKII (Caulino-Rocha et al.,

2022 [↗](#)). The relevant VIP receptor VPAC1 is known to exist in the amygdala (Joo et al., 2005 [↗](#); Boucher et al., 2021 [↗](#)). Thus, by inhibiting potentiation, VIP may change a Hebbian plasticity rule to a depression-dominated rule.

## Involvement of other brain structures

Studies using fear conditioning as a model of associative learning reveal that learning and expression of fear are not limited to the amygdala but involve a distributed network including the amygdala, the medial prefrontal cortex, and the hippocampus (Seidenbecher et al., 2003 [↗](#); Bocchio and Capogna, 2014 [↗](#); Courtin et al., 2014a [↗](#); Stujenske et al., 2014 [↗](#); Tovote et al., 2015 [↗](#); Karalis et al., 2016 [↗](#); Chen et al., 2021 [↗](#)). In our model, the fear-encoding neuron F fires for at least 13 seconds due to the US (first ~2 seconds), followed by the fear memory that could excite F in a similar way to US. This is suggested by the observation that during fear conditioning, animals are hyperactive for about 10 seconds after US presentation and then freeze while they are maintained in the box in which they received the shock (Hole and Lorens, 1975 [↗](#)). The medial prefrontal cortex and the hippocampus may provide the substrates for the continued firing of F needed for ECS to F potentiation after the 2-second US stimulation.

It has also been suggested that ventral tegmental area has a role in fear expression (Lesas et al., 2023 [↗](#)). Furthermore, it has been reported that the prelimbic cortex (PL) modulates the BLA SOM cells during fear retrieval, and the latter cells are crucial to discriminate non-threatening cues when desynchronized by the PL inputs (Stujenske et al., 2022 [↗](#)). Other brain structures, e.g., prefrontal cortex and hippocampus, have been documented to play a crucial role also in fear extinction, the paradigm following fear conditioning aimed at decrementing the conditioned fearful response through repeated presentations of the CS alone. As reported by several studies, fear extinction suppresses the fear memory through the acquisition of a distinct memory, instead of through the erasure of the fear memory itself (Harris et al., 2000 [↗](#); Bouton, 2002 [↗](#); Trouche et al., 2013 [↗](#); Thompson et al., 2018 [↗](#)). Davis et al., 2017 [↗](#) found a high theta rhythm following fear extinction that was associated with the suppression of threat in rodents. In the future, our BLA network will also include structures in the prefrontal cortex and hippocampus, thus allowing us to further study the role of rhythms in fear conditioning and extinction. We hypothesize that a new population of PV interneurons plays a crucial role in mediating competition between fearful memories, associated with a low theta rhythm, and safety memories, associated with a high theta rhythm; supporting experimental evidence is in (Lucas et al., 2016 [↗](#); Davis et al., 2017 [↗](#); Chen et al., 2022 [↗](#)).

## Comparison with other models

Our modeling approach aims at investigating the genesis and the functional role of rhythms in the amygdala fear circuit before, during, and after fear learning. Several computational models related to fear conditioning have been proposed in the last years, including connectionist models, firing rate models, and biophysically detailed ones (for a review see (Nair et al., 2016 [↗](#))). However, to the best of our knowledge, none focuses on rhythms generated by different kinds of interneurons. Among the biophysically detailed models, some tend to focus on the connectivity among a large number of similar neurons rather than the interactions among different kinds of neurons (Feng et al., 2016 [↗](#); Kim et al., 2016 [↗](#)). Our focus, using a smaller number of neurons, highlights the functional importance of the physiological differences among the different kinds of neurons in producing fine timing needed for plasticity. Feng et al., 2019 [↗](#) also suggests that the gamma in BLA is a PING; our paper looks at how this rhythm evolves during fear conditioning while also investigating interactions with other BLA rhythms.

The dynamics of the VIP cell play a central role in the plasticity we investigate. This is in contrast to the cortical model in (Veit et al., 2023 [↗](#)) for which VIP is essential for locally controlling gain and globally controlling coherence in gamma oscillations. In the model by Veit et al., 2023 [↗](#), the global control requires differences in long-range connectivity that are known to exist and are

inserted in the model by hypothesis. Our paper shows how more detailed biophysics produces rhythms among the interneurons used in (Veit et al., 2023) and how these rhythms can produce the plasticity needed to construct those differences in long-range connectivity. Thus, though (Veit et al., 2023) shows that rhythms are not needed for some kinds of control once connectivity is established, our paper suggests that the same set of interneurons, with more detailed physiology, can support the establishment of appropriate connectivity as well as the control described in (Veit et al., 2023). We note that Veit et al., 2023 deal with cortical networks, while our model describes BLA networks; however, it is known that these networks are structurally related (Sah et al., 2003; Tovote et al., 2015; Polepalli et al., 2020).

The study in (Grewe et al., 2017) suggests that fear conditioning induces both potentiation and depression among coactive excitatory neurons; coactivity was determined by calcium signaling and thus did not allow measurements of fine timing between spikes. In our model, depression happens in several circumstances: (1) in the absence of pauses of ECS and F firing and (2) in the absence of the fine timing provided by the PV neurons. This could happen among some cells responding to weaker sensory inputs that do not lead to pre-post timing with fear neurons. This timing could be modified by the “tri-conditional rule”, as suggested in (Grewe et al., 2017).

### Limitations and caveats

The use of small number of neurons raises the issue of model scalability. One way in which large models can be different from much smaller ones is in heterogeneity of the neurons of any given type. By using a network with a few neurons, we have begun the study of effects of heterogeneity. In general, the use of small numbers, which effectively assumes that each cell represents a synchronous subset of a larger population, replaces the use of gap-junctions that are known to exist in the cortex among VIP cells (Francavilla et al., 2018) as well as among SOM cells and among PV cells (Tremblay et al., 2016).

We do not explicitly model the biophysics of NMDA receptors. Rather, we model the effect of such receptors using the spike-timing-dependent plasticity resulting from such biophysics, as is commonly done when modeling STDP (Song et al., 2000). Also, our neurons are single-compartment, so do not build in the spatial structure known to exist on the dendrites (Blair et al., 2001; Bennett et al., 2019).

Our model assumes that initial stages of fear learning can be accomplished entirely within the amygdala, though it is known that other structures in the brain are important for modulating networks related to fear. Much of the work involving the prefrontal cortex and the hippocampus relates to fear extinction, which is not addressed in this paper.

### Summary and significance

We have shown how networks of amygdala neurons, including multiple types of interneurons, can work together to produce plasticity needed for fear learning. The coordination necessary to produce the plasticity requires the involvement of multiple rhythms. Thus, our paper both accounts for the experimental evidence showing such amygdala rhythms exist and points to their central role in the mechanisms of plasticity involved in associative learning. These mechanisms may be common to other types of associative learning, as similar interneuron subtypes and connectivity are ubiquitous in the cortex (Sah et al., 2003; Tovote et al., 2015; Polepalli et al., 2020).

## Acknowledgements

Research reported here was supported by the National Institute of Neurological Disorders and Stroke of the National Institute of Health under Award Number U01NS122082 to NK and DBA.

## Author contributions

Conceptualization, AC, DBA, MM, and NK; Methodology, AC, MM, and NK; Software, AC, and MM; Formal analysis, AC, and MM; Investigation, AC, MM, and MM; Data curation, AC; Writing – original draft, AC, MM, and NK; Visualization, AC, and DBA; Supervision, MM and NK; Funding acquisition: DBA and NK.

## Declaration of interests

The authors declare no competing interest.

## Materials and Methods

### Neuron model

Our network is made of interacting single-compartment neurons modeled using conductance-based models with Hodgkin-Huxley-type dynamics. The temporal voltage change of each neuron is described by:

$$c_m \frac{dV}{dt} = - \sum I_{membrane} - \sum I_{synaptic} + I_{app} + I_{noise},$$

where,  $c_m$  is the membrane capacitance, and  $I_{membrane}$  are the intrinsic membrane currents, which include a fast sodium current ( $I_{Na}$ ), a fast potassium current ( $I_K$ ), and a leak current ( $I_L$ ) for all neuron types. VIP interneurons additionally have a D-current, and SOM interneurons additionally have P and H-currents (Rotstein et al., 2005 [↗](#); Tort et al., 2007 [↗](#)). All these currents are discussed in more detail below, where we describe each neuron individually. The synaptic currents ( $I_{synaptic}$ ) take into account the input from the other neurons in the network and depend on the network connectivity and specific type of synaptic input, as discussed below. Finally, the background drive  $I_{app}$  is a constant term that determines the background excitation of a neuron, and  $I_{noise}$  corresponds to a Gaussian noise input with mean zero, standard deviation 1, and a specific amplitude for each neuronal cell type (specified below).

### Membrane currents

The membrane currents  $I_{Na}$ ,  $I_K$ , and  $I_L$  are modeled using Hodgkin-Huxley-type conductances formulated as:

$$\begin{aligned} I_{Na}(V, h) &= \bar{g}_{Na} m_{\infty}^3 h (V - E_{Na}) \\ \text{or, alternatively, } I_{Na}(V, h) &= \bar{g}_{Na} m^3 h (V - E_{Na}) \\ I_K(V, n) &= \bar{g}_K n^4 (V - E_K) \\ I_L(V) &= \bar{g}_L (V - E_L) \end{aligned} \tag{1}$$

Each membrane current has a constant maximal conductance  $\bar{g}_{channel}$  and a reversal potential  $E_{channel}$  (for  $channel = Na, K, \text{ or } L$ ). The activation ( $m$  and  $n$ ) and inactivation ( $h$ ) gating variables evolve in time according to:

$$\frac{dx}{dt} = \frac{x_{\infty} - x}{\tau_x}, \quad (2)$$

where  $x = m, n, h$ . The steady-state function ( $x_{\infty}$ ) and the time constant of decay ( $\tau_x$ ), which are taken from previous models (Mainen and Sejnowski, 1996; Olufsen et al., 2003), are formulated as rate functions for each opening ( $\alpha_x$ ) and closing ( $\beta_x$ ) of the ionic channel through:

$$x_{\infty} = \frac{\alpha_x}{\alpha_x + \beta_x} \quad (3)$$

$$\tau_x = \frac{1}{\alpha_x + \beta_x}.$$

The specific functions and constants for each cell type in the network are given below.

### Vasoactive intestinal peptide interneurons (VIP)

The membrane currents ( $I_{membrane}$ ) of the VIP interneurons consist of a fast sodium current ( $I_{Na}$ ) (described as in the first formulation of  $I_{Na}$  in Eq. (1)), a fast potassium current ( $I_K$ ), a leak current ( $I_L$ ), as in Eq. (1), and a potassium D-current ( $I_D$ ). The formulations of these currents were derived from a previous model of cortical interneurons (Golomb et al., 2007) and subsequently used to model striatal fast spiking interneurons (Sciamanna and Wilson, 2011; Chartove et al., 2020), which are reported below.

The maximal sodium conductance is  $\bar{g}_{Na} = 112.5 \text{ mS/cm}^2$  and the sodium reversal potential is  $E_{Na} = 50 \text{ mV}$ . The steady state functions for the sodium current activation ( $m$ ) and inactivation ( $h$ ) variables and  $h$  time constant ( $\tau_h$ ) are described by:

$$m_{\infty} = \frac{1}{1 + \exp[-(V + 24)/11.5]}$$

$$h_{\infty} = \frac{1}{1 + \exp[(V + 58.3)/6.7]}$$

$$\tau_h = 0.5 + \frac{14}{1 + \exp[(V + 60)/12]}.$$

The maximal conductance for the fast potassium channel is  $\bar{g}_K = 225 \text{ mS/cm}^2$  and the potassium reversal potential is  $E_K = -90 \text{ mV}$ . The fast potassium channel has no inactivation gates and two activation gates described as follows:

$$n_{\infty} = \frac{1}{1 + \exp[-(V + 12.4)/6.8]}$$

$$\tau_n = (0.087 + \frac{11.4}{1 + \exp[(V + 14.6)/8.6]})(0.087 + \frac{11.4}{1 + \exp[-(V - 1.3)/18.7]}).$$

The leak current ( $I_L$ ) has no gating variables. The maximal leak conductance is  $\bar{g}_L = 0.25 \text{ mS/cm}^2$  and the leak channel reversal potential is  $E_L = -70 \text{ mV}$ .

The fast-activating, slowly inactivating potassium D-current  $I_D$  is formulated as described in (Golomb et al., 2007 [↗](#)):

$$I_D(V, a, b) = \bar{g}_D a^3 b (V - E_K)$$

$$\frac{da}{dt} = \frac{a_\infty - a}{\tau_a}$$

$$\frac{db}{dt} = \frac{b_\infty - b}{\tau_b},$$

with maximal conductance  $\bar{g}_D = 3 \text{ mS/cm}^2$ . The steady state functions for the activation ( $a$ ) and inactivation ( $b$ ) variables are described as follows:

$$a_\infty = \frac{1}{1 + \exp [-(V + 50)/20]}$$

$$b_\infty = \frac{1}{1 + \exp [(V + 70)/6]},$$

while the time constant of the decay is  $\tau_a = 2 \text{ ms}$  for the activation gate and  $\tau_b = 150 \text{ ms}$  for the inactivation gate.

In the absence of US, the applied current  $I_{app}$  is set to  $4 \text{ } \mu\text{A/cm}^2$ . When US is present,  $I_{app} = 5 \text{ } \mu\text{A/cm}^2$ . The Gaussian noise ( $I_{noise}$ ) has mean 0, standard deviation 1, and an amplitude of  $5\sqrt{\delta t}$ , where  $\delta t = 0.05 \text{ ms}$  corresponds to the time step of integration in our simulations.

### Somatostatin-positive interneurons (SOM)

The membrane currents ( $I_{membrane}$ ) of the SOM interneurons consist of a fast sodium current ( $I_{Na}$ ) (described as in the second formulation of  $I_{Na}$  in Eq. (1) [↗](#)), a fast potassium current ( $I_K$ ), and a leak current ( $I_L$ ) as in Eq.(1), along with an H-current ( $I_H$ ) and NaP-current ( $I_P$ ). The formulations of these currents were taken from previous models of the oriens lacunosum-moleculare (SOM-positive O-LM) cells in the hippocampus (Rotstein et al., 2005 [↗](#); Tort et al., 2007 [↗](#)) and are reported below.

The maximal sodium conductance is  $\bar{g}_{Na} = 52 \text{ mS/cm}^2$  and the sodium reversal potential is  $E_{Na} = 55 \text{ mV}$ . The rate functions for the sodium current activation ( $m$ ) and inactivation ( $h$ ) variables in Eqs. (2-3) are formulated as follows:

$$\alpha_m = \frac{-0.1(V + 23)}{\exp [-0.1(V + 23) - 1]}$$

$$\beta_m = 4 \exp [-(V + 48)/18]$$

$$\alpha_h = 0.07 \exp [-(V + 37)/20]$$

$$\beta_h = \frac{1}{\exp [-0.1(V + 7) + 1]}.$$

The maximal potassium conductance is  $\bar{g}_K = 11 \text{ mS/cm}^2$  and the potassium reversal potential is  $E_K = -90 \text{ mV}$ . The rate functions for the potassium current activation variable ( $n$ ) are formulated as follows:

$$\alpha_n = \frac{-0.01(V + 27)}{\exp[-0.1(V + 27) - 1]}$$

$$\beta_n = 0.125 \exp[-(V + 37)/80].$$

The leak current ( $I_L$ ) has no gating variables. The maximal leak conductance is  $\bar{g}_L = 0.62 \text{ mS/cm}^2$  and the leak channel reversal potential is  $E_L = -65 \text{ mV}$ .

The slow hyperpolarization-activated mixed cation current  $I_H$  is formulated as described in (Rotstein et al., 2005 [↗](#)):

$$I_H(V, h^f, h^s) = \bar{g}_H(0.65h^f + 0.35h^s)(V - E_H)$$

$$\frac{dh^f}{dt} = \frac{h_\infty^f - h^f}{\tau_{hf}}$$

$$\frac{dh^s}{dt} = \frac{h_\infty^s - h^s}{\tau_{hs}},$$

with maximal conductance  $\bar{g}_H = 1.45 \text{ mS/cm}^2$  and  $E_H = -20 \text{ mV}$ . The steady state functions for the  $h^f$  and  $h^s$  variables and their time constant of decay are described as follows:

$$h_\infty^f = \frac{1}{1 + \exp[(V + 79.2)/9.78]}$$

$$\tau_{hf} = \frac{0.51}{\exp[(V - 1.7)/10] + -\exp[(V + 340)/52]} + 1$$

$$h_\infty^s = \frac{1}{1 + \exp[(V + 2.83)/15.9]^{58}}$$

$$\tau_{hs} = \frac{5.6}{\exp[(V - 1.7)/14] + -\exp[-(V + 260)/43]} + 1.$$

The persistent sodium current  $I_P$  is formulated as described in (Rotstein et al., 2005 [↗](#), 2006 [↗](#)):

$$I_P = \bar{g}_P p(V - E_{Na}).$$

The maximal persistent sodium conductance is  $\bar{g}_p = 0.5 \text{ mS/cm}^2$  and the sodium reversal potential is, as stated above,  $E_{Na} = 55 \text{ mV}$ . The steady state function for the persistent sodium current  $I_p$  ( $p_\infty$ ) and the time constant ( $\tau_p$ ) are described by:

$$p_\infty = \frac{1}{1 + \exp [-(V + 38)/6.5]}$$

$$\tau_p = 0.15.$$

Throughout all simulations, the applied current  $I_{app}$  is set to  $0.1 \mu\text{A/cm}^2$ . The Gaussian noise ( $I_{noise}$ ) has mean 0, standard deviation 1, and an amplitude of  $4\sqrt{\delta t}$ , where  $\delta t = 0.05 \text{ ms}$  corresponds to the time step of integration in our simulations. We note that the persistent sodium current can be replaced by an A-current to produce a high theta rhythm (Glovelli et al., 2005 [\[1\]](#)).

### Parvalbumin-positive interneurons (PV)

The membrane currents ( $I_{membrane}$ ) of the PV interneurons consist of only a fast sodium current ( $I_{Na}$ ) (described as in the second formulation of  $I_{Na}$  in Eq. (1) [\[1\]](#)), a fast potassium current ( $I_K$ ), and a leak current ( $I_L$ ), as in Eq. (1) [\[1\]](#).

The maximal sodium conductance is  $\bar{g}_{Na} = 100 \text{ mS/cm}^2$  and the sodium reversal potential is  $E_{Na} = 50 \text{ mV}$ . The rate functions for the sodium current activation ( $m$ ) and inactivation ( $h$ ) variables are formulated as follows:

$$\alpha_m = \frac{0.32(V + 54)}{1 - \exp [-(V + 54)/4]}$$

$$\beta_m = \frac{0.28(V + 27)}{\exp[(V + 27)/5] - 1}$$

$$\alpha_h = 0.128 \exp [-(V + 50)/18]$$

$$\beta_h = \frac{4}{1 + \exp [-(V + 27)/5]}.$$

The maximal potassium conductance is  $\bar{g}_K = 80 \text{ mS/cm}^2$  and the potassium reversal potential is  $E_K = -100 \text{ mV}$ . The rate functions for the potassium current activation ( $n$ ) variables are formulated as follows:

$$\alpha_n = \frac{0.032(V + 52)}{1 - \exp [-(V + 52)/5]}$$

$$\beta_n = 0.5 \exp [-(V + 57)/40].$$

The leak current ( $I_L$ ) has no gating variables. The maximal leak conductance is  $\bar{g}_L = 0.1 \text{ mS/cm}^2$  and the leak channel reversal potential is  $E_L = -67 \text{ mV}$ . Throughout all the simulations,  $I_{app} = 0 \mu\text{A/cm}^2$ . The Gaussian noise ( $I_{noise}$ ) has mean 0, standard deviation 1, and an amplitude of  $4\sqrt{\delta t}$ , where  $\delta t = 0.05 \text{ ms}$  corresponds to the time step of integration in our simulations.

## Excitatory projection neurons (ECS and F)

The membrane currents ( $I_{membrane}$ ) of ECS and F consist of a fast sodium current ( $I_{Na}$ ) (described as in the first formulation of  $I_{Na}$  in Eq. (1) [↗](#)), a fast potassium current ( $I_K$ ), and a leak current ( $I_L$ ) as in Eq. (1) [↗](#).

The maximal sodium conductance is  $\bar{g}_{Na} = 100 \text{ mS/cm}^2$  and the sodium reversal potential is  $E_{Na} = 50 \text{ mV}$ . The rate functions for the sodium current activation ( $m$ ) and inactivation ( $h$ ) variables are formulated as follows:

$$\alpha_m = \frac{0.1(V + 35)}{1 - \exp[-(V + 35)/10]}$$

$$\beta_m = 4 \exp[-(V + 60)/18]$$

$$\alpha_h = 0.07 \exp[-(V + 58)/20]$$

$$\beta_h = \frac{1}{\exp[-0.1(V + 28)] + 1}$$

The maximal potassium conductance is  $\bar{g}_K = 80 \text{ mS/cm}^2$  and the potassium reversal potential is  $E_K = -100 \text{ mV}$ . The rate functions for the potassium current activation ( $n$ ) variables are formulated as follows:

$$\alpha_n = \frac{-0.01(V + 34)}{\exp[-0.1(V + 34) - 1]}$$

$$\beta_n = 0.125 \exp[-(V + 44)/80].$$

The leak current ( $I_0$ ) has no gating variables. The maximal leak conductance is  $\bar{g}_L = 0.1 \text{ mS/cm}^2$  and the leak channel reversal potential is  $E_L = -67 \text{ mV}$ . The formulations of these currents were taken from the description of excitatory/inhibitory neurons presented in (Zhou et al., 2018) [↗](#).

When neither US nor CS are injected, the applied current  $I_{app,F}$  is set to  $0.35 \mu\text{A/cm}^2$  and  $I_{app,ECS}$  is set to  $0.45 \mu\text{A/cm}^2$ . By contrast,  $I_{app,F}$  is set to  $0.5 \mu\text{A/cm}^2$  when US is injected. For both ECS and F, the Gaussian noise ( $I_{noise}$ ) has mean 0, standard deviation 1, and an amplitude of  $4\sqrt{\delta t}$ , where  $\delta t = 0.05 \text{ ms}$  corresponds to the time step of integration in our simulations.

## Conditioned and unconditioned stimuli

The conditioned (CS) and unconditioned (US) stimuli affect specific cell types according to the fear conditioning phase. CS consists of a Poisson spike train ( $\lambda = 800$ ) that excites an auxiliary excitatory neuron (described by the same equations used for ECS in the previous section). The auxiliary excitatory neuron excites both ECS and PV and makes them fire, in isolation, at  $\sim 50 \text{ Hz}$ . The maximal AMPA conductance from the auxiliary excitatory neuron to PV and ECS is  $\bar{g}_e = 0.2 \text{ mS/cm}^2$  (see the next paragraph for a description of the AMPA synapses). Many  $\bar{g}_e$  AMPA conductance values from the auxiliary excitatory neuron to PV (spanning from  $0.01 \text{ mS/cm}^2$  to  $0.2 \text{ mS/cm}^2$ ) have been considered to make Fig. S3B. Similarly, US ( $\lambda = 800$ , independent of CS) affects an auxiliary excitatory neuron that makes F fire in isolation fires at  $\sim 50 \text{ Hz}$ . The maximal

AMPA conductance from the auxiliary excitatory neuron to F is  $\bar{g}_e = 0.2 \text{ mS/cm}^2$  (see the next paragraph for a description of the AMPA synapses). Finally, US influences VIP activity by increasing its  $I_{app}$  set to  $5 \mu\text{A/cm}^2$ .

## Network connectivity and synaptic currents

We modeled the network connectivity as presented in [Fig. 2B](#), derived from ([Krabbe et al., 2019](#)). We have a total of 9 types of projections between neurons: 6 inhibitory (VIP → PV, VIP → SOM, PV → F, PV → ECS, SOM → F, SOM → ECS), 3 excitatory (ECS → F, F → PV, F → VIP).

All inhibitory synapses are described as GABA<sub>A</sub> currents ( $I_{GABA_A}$ ) using a Hodgkin-Huxley-type conductance, as formulated in ([Olufsen et al., 2003](#)):

$$I_{GABA_A} = \bar{g}_i s_i (V - E_i).$$

The maximal GABA<sub>A</sub> conductance VIP → PV is  $\bar{g}_i = 1/N_{VIP} \text{ mS/cm}^2$ , VIP → SOM is  $\bar{g}_i = 1/N_{SOM} \text{ mS/cm}^2$ , PV → F is  $\bar{g}_i = 0.5/N_{PV} \text{ mS/cm}^2$ , PV → ECS is  $\bar{g}_i = 0.4/N_{PV} \text{ mS/cm}^2$ , SOM → F is  $\bar{g}_i = 0.4/N_{SOM} \text{ mS/cm}^2$ , and SOM → ECS is  $\bar{g}_i = 0.4/N_{SOM} \text{ mS/cm}^2$ , where  $N_{VIP}$ ,  $N_{PV}$ ,  $N_{SOM}$  are the number of VIP, PV, and SOM cells, respectively, in the network. The GABA<sub>A</sub> current reversal potential ( $E_i$ ) is set to  $-80 \text{ mV}$ . The variable  $s_i$  represents the gating variable for inhibitory GABA<sub>A</sub> synaptic transmission, where  $i$  stands for inhibitory synapse. The contribution of an inhibitory synapse to a specific postsynaptic inhibitory neuron  $j$  in the network takes the following form:

$$s_i = \sum_k S_{i_k i_j}. \quad (4)$$

The contribution to a specific postsynaptic excitatory neuron  $m$  in the network, reads as follows:

$$s_i = \sum_k S_{i_k e_m}, \quad (5)$$

where  $k$  indexes the presynaptic inhibitory neurons. The variable  $S_{i_k i_j}$  in [Eq. \(4\)](#) describes the kinetics of the gating variables from the inhibitory presynaptic neuron  $k^{\text{th}}$  to the inhibitory postsynaptic neuron  $j$ . This variable evolves in time according to:

$$\frac{dS_{i_k i_j}}{dt} = g_{GABA_A}(V_k) (1 - S_{i_k i_j}) - \frac{S_{i_k i_j}}{\tau_{i_k}}.$$

Similarly, the kinetics of the gating activation variable  $S_{i_k e_m}$  in [Eq. \(5\)](#) from the  $k^{\text{th}}$  interneuron to the postsynaptic excitatory neuron  $m$  is formulated as:

$$\frac{dS_{i_k e_m}}{dt} = g_{GABA_A}(V_k) (1 - S_{i_k e_m}) - \frac{S_{i_k e_m}}{\tau_{i_k}}.$$

The GABAa decay time constant ( $\tau_{I_k}$ ) is a constant that depends on the type of presynaptic interneuron. The rate functions for the open state of the GABAa receptor ( $g_{GABAa}(V_k)$ ) has a specific form based on the presynaptic cell type  $k$ . More specifically,

$$\text{For } k = \text{VIP: } g_{GABAa}(V_k) = 2(1 + \tanh(\frac{V_k}{4})), \tau_{I_k} = 10 \text{ ms}$$

$$\text{For } k = \text{PV: } g_{GABAa}(V_k) = \frac{15}{2}(1 + \tanh(\frac{V_k}{0.1})), \tau_{I_k} = 8.3 \text{ ms}$$

$$\text{For } k = \text{SOM: } g_{GABAa}(V_k) = \frac{5}{2}(1 + \tanh(\frac{V_k}{0.1})), \tau_{I_k} = 20 \text{ ms.}$$

All excitatory synapses are described as AMPA currents ( $I_{AMPA}$ ) using a Hodgkin-Huxley-type conductance, as formulated in (Olufsen et al., 2003 [↗](#)):

$$I_{AMPA} = \bar{g}_e s_e (V - E_e).$$

At the beginning of the fear conditioning paradigm there is no connection from ECS to F, i.e., the maximal AMPA conductance ECS  $\rightarrow$  F is  $\bar{g}_e = 0 \text{ mS/cm}^2$ . Since ECS to F is a plastic connection (see paragraph related to synaptic plasticity), it evolves over time up to a maximum of  $\bar{g}_e = 0.18 \text{ mS/cm}^2$ . The maximal AMPA conductance F  $\rightarrow$  PV is  $\bar{g}_e = 0.5 \text{ mS/cm}^2$ , and F  $\rightarrow$  VIP is  $\bar{g}_e = 0.01 \text{ mS/cm}^2$ . In the case of the plastic F to VIP cell connections (see Supplementary Information), the F  $\rightarrow$  VIP conductances evolve over time up to a maximum of  $\bar{g}_e = 0.04 \text{ mS/cm}^2$ . The AMPA current reversal potential ( $E_e$ ) is set to  $0 \text{ mV}$ .

The variable  $s_e$  represents the gating variable for excitatory AMPA synaptic transmission, where  $e$  stands for excitatory synapse. For a specific postsynaptic excitatory neuron  $m$  in the network:

$$s_e = \sum_k S_{e_k e_m}.$$

For a specific postsynaptic inhibitory neuron  $j$  in the network:

$$s_i = \sum_k S_{e_k i_j},$$

where  $k$  indexes the presynaptic excitatory neurons.

The variable  $S_{e_k e_m}$  describes the kinetics of the gating variables from the excitatory presynaptic neuron  $k^{th}$  to the excitatory postsynaptic neuron  $m$ . This variable evolves in time according to:

$$\frac{dS_{e_k e_m}}{dt} = g_{AMPA}(V_k)(1 - S_{e_k e_m}) - \frac{S_{e_k e_m}}{\tau_e}.$$

Similarly, the kinetics of the synaptic activation variable of the  $k^{\text{th}}$  excitatory neuron to the inhibitory neuron  $j$  is denoted by  $S_{ekij}$  and is formulated as:

$$\frac{dS_{ekij}}{dt} = g_{AMPA}(V_k) \left(1 - S_{ekij}\right) - \frac{S_{ekij}}{\tau_e}.$$

The time-constant of decay for the AMPA synapse is  $\tau_e = 2 \text{ ms}$ . The rate functions for the open state of the AMPA receptor ( $g_{AMPA}(V_k)$ ) follows the mathematical formulation:

$$g_{AMPA}(V_k) = 5 \left(1 + \tanh\left(\frac{V_k}{4}\right)\right), k = F, ECS.$$

### Synaptic plasticity

Fear conditioning is a paradigm able to create associative learning between the neutral (CS) and the aversive (US) stimuli. Synaptic plasticity is thought to be at the basis of associative learning. In our work, synaptic plasticity takes the form of spike-timing-dependent plasticity (Song et al., 2000; Lee et al., 2009), where synaptic modifications are enforced at the synapse from ECS to F at each presynaptic (ECS) and postsynaptic (F) neuron spikes. Synaptic modification is generated in the model through two auxiliary functions: P, used for potentiation, and M, used for depression, as in standard STDP models. The major difference between our use of STDP and some others is that, for each pre-synaptic spike, we take into account all the post-synaptic spikes with which it could potentially interact; similarly for each post-synaptic spike, we take into account all presynaptic spikes. P and M are initialized at zero and are updated at each presynaptic and postsynaptic neuron spike, respectively. Between spikes, they exponentially decay to zero (see Fig. S1). The update is described as follows. At each postsynaptic neuron (F) spike,  $M(t)$  is decremented by an amount  $A_- = 0.005$ , i.e.,  $M(t) = M(t) - A_-$ . At each presynaptic neuron (ECS) spike,  $P(t)$  is incremented by an amount  $A_+ = 0.005$ , i.e.,  $P(t) = P(t) + A_+$  (Fig.S1A). This Hebbian plasticity rule is depression-dominant when  $A_+ = A_-$  and  $\tau_+ < \tau_-$ , as formulated in this work. The exponential decay is described by the following equations:

$$\tau_- \frac{dM}{dt} = -M$$

$$\tau_+ \frac{dP}{dt} = -P,$$

with  $\tau_- = 28 \text{ ms}$  and  $\tau_+ = 14 \text{ ms}$ . Every time the synapse receives an ECS action potential at time  $t$ , its maximal conductance is weakened according to  $\bar{g} = \bar{g} + M(t)$ . If  $\bar{g} < 0$ ,  $\bar{g}$  is set to zero. If F fires an action potential at time  $t$ , the synapse maximal conductance is strengthened according to  $\bar{g} = \bar{g} + P(t)$ . If this strengthening makes  $\bar{g} > \bar{g}_{max}$ , then  $\bar{g}$  is set to  $\bar{g}_{max} = 0.18 \text{ mS/cm}^2$  (see Fig. S1A, right, for an example). See Supplementary Information for a visualization of M and P and consequences of the depression-dominated rule.

In the Supplementary Information we introduce a plastic connection from the fear neuron F to the VIP interneurons. For that specific synapse,  $A_+ = 0.00065$  and  $A_- = 0.0003$ , while the decay time constants are as above. In this case, the rule is not depression-dominant.

## Model simulations

Our network models were programmed in C++ and compiled using g++ compiler (Apple clang version 14.0.0) on macOS Monterey version 12.5.1. The differential equations were integrated using a fourth-order Runge Kutta algorithm. The integration time step was 0.05 ms. Model output is graphed and analyzed using MATLAB, Version R2022a. Simulation codes are made freely available (see Resource Availability section).

## Local field potentials and spectral analysis

### Modeling LFP

One measure of neuronal population activity in the BLA is the LFP. It has been suggested that inhibitory synaptic currents represent a major contribution to LFP in the hippocampus and the cortex because of the neurons arranged in a laminar way (Bazelot et al., 2010 [↗](#); Teleńczuk et al., 2017 [↗](#), 2020 [↗](#)). By contrast, LFP in brain regions with no laminar structure (as the BLA), may be generated by localized excitatory inputs and intrinsic membrane currents (Reimann et al., 2013 [↗](#); Tanaka and Nakamura, 2019 [↗](#)). For this reason, we model the LFP as the sum of all synaptic AMPA currents in the pyramidal cells, along with the D-current in the VIP interneurons, and NaP-current and H-current in SOM interneurons.

### Spectral analysis

Stationarity of the network before and after fear conditioning is ensured after 2000 ms. Thus, to ensure elimination of transients due to initial conditions, we discard the first 2000 ms of LFP signals. LFP's power spectra are calculated using the Thomson's multitaper power spectral density estimate (MATLAB function pmtm) (Bokil et al., 2007 [↗](#)) for frequencies ranging from 0.1 – 70 Hz. Analysis codes are made freely available (see Resource Availability section).

## Resource availability

### Data and code availability

The computer simulation code created for this paper, as well as the code to make the figures presented, are available online at [https://github.com/annacatt/Basolateral\\_amygdala\\_oscillations\\_enable\\_fear\\_learning\\_in\\_a\\_biophysical\\_model](https://github.com/annacatt/Basolateral_amygdala_oscillations_enable_fear_learning_in_a_biophysical_model) [↗](#). The simulated data that support the findings of this study are available at <https://datadryad.org/stash/share/FCSYmUOhwforkleWFwIKW2hhmu2XXA7hsvsYbWnQGCU> [↗](#) (the following DOI will be active after publication: <https://doi.org/10.5061/dryad.pvmcvdnr2> [↗](#))

## References

- Abbott LF, Nelson SB (2000) **Synaptic plasticity: taming the beast** *Nat Neurosci* **3**:1178–1183
- Agoston DV, Conlon JM, Whittaker VP (1988) **Selective depletion of the acetylcholine and vasoactive intestinal polypeptide of the guinea-pig myenteric plexus by differential mobilization of distinct transmitter pools** *Exp Brain Res* **72**:535–542
- Agoston DV, Lisziewicz J (1989) **Calcium uptake and protein phosphorylation in myenteric neurons, like the release of vasoactive intestinal polypeptide and acetylcholine, are frequency dependent** *J Neurochem* **52**:1637–1640
- Bayraktar T, Staiger JF, Acsady L, Cozzari C, Freund TF, Zilles K (1997) **Co-localization of vasoactive intestinal polypeptide, gamma-aminobutyric acid and choline acetyltransferase in neocortical interneurons of the adult rat** *Brain Res* **757**:209–217
- Bazelot M, Dinocourt C, Cohen I, Miles R (2010) **Unitary inhibitory field potentials in the CA3 region of rat hippocampus** *J Physiol* **588**:2077–2090
- Bennett MR, Farnell L, Gibson WG, Lagopoulos J (2019) **A model of amygdala function following plastic changes at specific synapses during extinction** *Neurobiology of Stress* **10**
- Bi G, Poo M (2001) **Synaptic modification by correlated activity: Hebb's postulate revisited** *Annu Rev Neurosci* **24**:139–166
- Bienvenu TCM, Busti D, Magill PJ, Ferraguti F, Capogna M (2012) **Cell-Type-Specific Recruitment of Amygdala Interneurons to Hippocampal Theta Rhythm and Noxious Stimuli In Vivo** *Neuron* **74**:1059–1074
- Blair HT, Schafe GE, Bauer EP, Rodrigues SM, LeDoux JE (2001) **Synaptic Plasticity in the Lateral Amygdala: A Cellular Hypothesis of Fear Conditioning** *Learn Mem* **8**:229–242
- Bocchio M, Capogna M (2014) **Oscillatory substrates of fear and safety** *Neuron* **83**:753–755
- Bocchio M, Nabavi S, Capogna M (2017) **Synaptic Plasticity, Engrams, and Network Oscillations in Amygdala Circuits for Storage and Retrieval of Emotional Memories** *Neuron* **94**:731–743
- Bokil H, Purpura K, Schoffelen J-M, Thomson D, Mitra P (2007) **Comparing spectra and coherences for groups of unequal size** *J Neurosci Methods* **159**:337–345
- Börger C, Epstein S, Kopell NJ (2005) **Background gamma rhythmicity and attention in cortical local circuits: a computational study** *Proc Natl Acad Sci U S A* **102**:7002–7007
- Boucher MN, May V, Braas KM, Hammack SE (2021) **PACAP orchestration of stress-related responses in neural circuits** *Peptides* **142**
- Bouton ME (2002) **Context, ambiguity, and unlearning: sources of relapse after behavioral extinction** *Biol Psychiatry* **52**:976–986
- Bouton ME (2004) **Context and behavioral processes in extinction** *Learn Mem* **11**:485–494

- Caporale N, Dan Y (2008) **Spike Timing-Dependent Plasticity: A Hebbian Learning Rule** *Annu Rev Neurosci* **31**:25–46
- Caulino-Rocha A, Rodrigues NC, Ribeiro JA, Cunha-Reis D (2022) **Endogenous VIP VPAC1 Receptor Activation Modulates Hippocampal Theta Burst Induced LTP: Transduction Pathways and GABAergic Mechanisms** *Biology (Basel)* **11**
- Chartove JAK, McCarthy MM, Pittman-Polletta BR, Kopell NJ (2020) **A biophysical model of striatal microcircuits suggests gamma and beta oscillations interleaved at delta/theta frequencies mediate periodicity in motor control** *PLoS Comput Biol* **16**
- Chen S, Tan Z, Xia W, Gomes CA, Zhang X, Zhou W, Liang S, Axmacher N, Wang L (2021) **Theta oscillations synchronize human medial prefrontal cortex and amygdala during fear learning** *Sci Adv* **7**
- Chen Y-H, Hu N-Y, Wu D-Y, Bi L-L, Luo Z-Y, Huang L, Wu J-L, Wang M-L, Li J-T, Song Y-L, Zhang S-R, Jie W, Li X-W, Zhang S-Z, Yang J-M, Gao T-M (2022) **PV network plasticity mediated by neuregulin1-ErbB4 signalling controls fear extinction** *Mol Psychiatry* **27**:896–906
- Courtin J, Chaudun F, Rozeske RR, Karalis N, Gonzalez-Campo C, Wurtz H, Abdi A, Baufreton J, Bienvenu TCM, Herry C (2014) **Prefrontal parvalbumin interneurons shape neuronal activity to drive fear expression** *Nature* **505**:92–96
- Courtin J, Karalis N, Gonzalez-Campo C, Wurtz H, Herry C (2014) **Persistence of amygdala gamma oscillations during extinction learning predicts spontaneous fear recovery** *Neurobiology of Learning and Memory* **113**:82–89
- Davis P, Zaki Y, Maguire J, Reijmers LG (2017) **Cellular and oscillatory substrates of fear extinction learning** *Nat Neurosci* **20**:1624–1633
- Fanselow MS, LeDoux JE (1999) **Why we think plasticity underlying Pavlovian fear conditioning occurs in the basolateral amygdala** *Neuron* **23**:229–232
- Feldman DE (2012) **The Spike-Timing Dependence of Plasticity** *Neuron* **75**:556–571
- Feng F, Headley DB, Amir A, Kanta V, Chen Z, Paré D, Nair SS (2019) **Gamma Oscillations in the Basolateral Amygdala: Biophysical Mechanisms and Computational Consequences** *eNeuro* **6**
- Feng F, Samarth P, Paré D, Nair SS (2016) **Mechanisms underlying the formation of the amygdalar fear memory trace: A computational perspective** *Neuroscience* **322**:370–376
- Francavilla R, Villette V, Luo X, Chamberland S, Muñoz-Pino E, Camiré O, Wagner K, Kis V, Somogyi P, Topolnik L (2018) **Connectivity and network state-dependent recruitment of long-range VIP-GABAergic neurons in the mouse hippocampus** *Nat Commun* **9**
- Gillies MJ, Traub RD, LeBeau FEN, Davies CH, Gloveli T, Buhl EH, Whittington MA (2002) **A model of atropine-resistant theta oscillations in rat hippocampal area CA1** *J Physiol* **543**:779–793
- Gloveli T, Dugladze T, Rotstein HG, Traub RD, Monyer H, Heinemann U, Whittington MA, Kopell NJ (2005) **Orthogonal arrangement of rhythm-generating microcircuits in the hippocampus** *Proc Natl Acad Sci U S A* **102**:13295–13300

- Golomb D, Donner K, Shacham L, Shlosberg D, Amitai Y, Hansel D (2007) **Mechanisms of Firing Patterns in Fast-Spiking Cortical Interneurons** Graham LJ *PLoS Comput Biol* **3**
- Grewe BF, Gründemann J, Kitch LJ, Lecoq JA, Parker JG, Marshall JD, Larkin MC, Jercog PE, Grenier F, Li JZ, Lüthi A, Schnitzer MJ (2017) **Neural ensemble dynamics underlying a long-term associative memory** *Nature* **543**:670–675
- Harris JA, Jones ML, Bailey GK, Westbrook RF (2000) **Contextual control over conditioned responding in an extinction paradigm** *J Exp Psychol Anim Behav Process* **26**:174–185
- Hole K, Lorens SA (1975) **Response to electric shock in rats: effects of selective midbrain raphe lesions** *Pharmacol Biochem Behav* **3**:95–102
- Johansen JP, Diaz-Mataix L, Hamanaka H, Ozawa T, Ycu E, Koivumaa J, Kumar A, Hou M, Deisseroth K, Boyden ES, LeDoux JE (2014) **Hebbian and neuromodulatory mechanisms interact to trigger associative memory formation** *Proc Natl Acad Sci U S A* **111**:E5584–5592
- Joo KM, Chung YH, Lim H, Lee KH, Cha CI (2005) **Reduced immunoreactivities of a vasoactive intestinal peptide and pituitary adenylate cyclase-activating polypeptide receptor (VPAC1 receptor) in the cerebral cortex, hippocampal region, and amygdala of aged rats** *Brain Res* **1064**:166–172
- Karalis N, Dejean C, Chaudun F, Khoder S, Rozeske RR, Wurtz H, Bagur S, Benchenane K, Sirota A, Courtin J, Herry C (2016) **4-Hz oscillations synchronize prefrontal-amygdala circuits during fear behavior** *Nat Neurosci* **19**:605–612
- Kim D, Samarth P, Feng F, Pare D, Nair SS (2016) **Synaptic competition in the lateral amygdala and the stimulus specificity of conditioned fear: a biophysical modeling study** *Brain Struct Funct* **221**:2163–2182
- Krabbe S, Gründemann J, Lüthi A (2018) **Amygdala Inhibitory Circuits Regulate Associative Fear Conditioning** *Biological Psychiatry* **83**:800–809
- Krabbe S, Paradiso E, d’Aquin S, Bitterman Y, Courtin J, Xu C, Yonehara K, Markovic M, Müller C, Eichlisberger T, Gründemann J, Ferraguti F, Lüthi A (2019) **Adaptive disinhibitory gating by VIP interneurons permits associative learning** *Nat Neurosci* **22**:1834–1843
- Lee S, Sen K, Kopell N (2009) **Cortical gamma rhythms modulate NMDAR-mediated spike timing dependent plasticity in a biophysical model** *PLoS Comput Biol* **5**
- Lesas J, Pierre F, Herry C, Dejean C (2023) **Lesas J, Pierre F, Herry C, Dejean C (2023) Dopamine enhances population coding of fear in prefrontal cortex. :2023.01.17.524376 Available at: <https://www.biorxiv.org/content/10.1101/2023.01.17.524376v1> x[Accessed April 27, 2023].**
- Lucas EK, Jegarl AM, Morishita H, Clem RL (2016) **Multimodal and Site-Specific Plasticity of Amygdala Parvalbumin Interneurons after Fear Learning** *Neuron* **91**:629–643
- Maccaferri G, McBain CJ (1996) **The hyperpolarization-activated current (I<sub>h</sub>) and its contribution to pacemaker activity in rat CA1 hippocampal stratum oriens-alveus interneurons** *J Physiol* **497**:119–130

- Muller JF, Mascagni F, McDonald AJ (2006) **Pyramidal cells of the rat basolateral amygdala: synaptology and innervation by parvalbumin-immunoreactive interneurons** *J Comp Neurol* **494**:635–650
- Muller JF, Mascagni F, McDonald AJ (2007) **Postsynaptic targets of somatostatin-containing interneurons in the rat basolateral amygdala** *J Comp Neurol* **500**:513–529
- Nabavi S, Fox R, Proulx CD, Lin JY, Tsien RY, Malinow R (2014) **Engineering a memory with LTD and LTP** *Nature* **511**:348–352
- Nair SS, Paré D, Vicentic A (2016) **Biologically based neural circuit modelling for the study of fear learning and extinction** *NPJ Sci Learn* **1**
- Olufsen MS, Whittington MA, Camperi M, Kopell N (2003) **New roles for the gamma rhythm: population tuning and preprocessing for the Beta rhythm** *J Comput Neurosci* **14**:33–54
- Perrenoud Q, Cardin JA (2023) **Putting the brakes on synchrony: VIP interneurons tune visually evoked rhythmic activity** *Neuron* **111**:297–299
- Phelps EA, LeDoux JE (2005) **Contributions of the amygdala to emotion processing: from animal models to human behavior** *Neuron* **48**:175–187
- Polepalli JS, Gooch H, Sah P (2020) **Diversity of interneurons in the lateral and basal amygdala** *npj Sci Learn* **5**:1–9
- Porter JT, Cauli B, Staiger JF, Lambolez B, Rossier J, Audinat E (1998) **Properties of bipolar VIPergic interneurons and their excitation by pyramidal neurons in the rat neocortex** *Eur J Neurosci* **10**:3617–3628
- Rainnie DG, Mania I, Mascagni F, McDonald AJ (2006) **Physiological and morphological characterization of parvalbumin-containing interneurons of the rat basolateral amygdala** *J Comp Neurol* **498**:142–161
- Reimann MW, Anastassiou CA, Perin R, Hill SL, Markram H, Koch C (2013) **A biophysically detailed model of neocortical local field potentials predicts the critical role of active membrane currents** *Neuron* **79**:375–390
- Rogan MT, Stäubli UV, LeDoux JE (1997) **Fear conditioning induces associative long-term potentiation in the amygdala** *Nature* **390**:604–607
- Rotstein HG, Oppermann T, White JA, Kopell N (2006) **The dynamic structure underlying subthreshold oscillatory activity and the onset of spikes in a model of medial entorhinal cortex stellate cells** *J Comput Neurosci* **21**:271–292
- Rotstein HG, Pervouchine DD, Acker CD, Gillies MJ, White JA, Buhl EH, Whittington MA, Kopell N (2005) **Slow and fast inhibition and an H-current interact to create a theta rhythm in a model of CA1 interneuron network** *J Neurophysiol* **94**:1509–1518
- Rumpel S, LeDoux J, Zador A, Malinow R (2005) **Postsynaptic receptor trafficking underlying a form of associative learning** *Science* **308**:83–88
- Sah P, Faber ESL, Lopez De Armentia M, Power J (2003) **The amygdaloid complex: anatomy and physiology** *Physiol Rev* **83**:803–834

- Sah P, Westbrook RF, Lüthi A (2008) **Fear conditioning and long-term potentiation in the amygdala: what really is the connection?** *Ann N Y Acad Sci* **1129**:88–95
- Saraga F, Wu CP, Zhang L, Skinner FK (2003) **Active dendrites and spike propagation in multicompartiment models of oriens-lacunosum/moleculare hippocampal interneurons** *J Physiol* **552**:673–689
- Schafe GE, Atkins CM, Swank MW, Bauer EP, Sweatt JD, LeDoux JE (2000) **Activation of ERK/MAP kinase in the amygdala is required for memory consolidation of pavlovian fear conditioning** *J Neurosci* **20**:8177–8187
- Sciamanna G, Wilson CJ (2011) **The ionic mechanism of gamma resonance in rat striatal fast-spiking neurons** *J Neurophysiol* **106**:2936–2949
- Seidenbecher T, Laxmi TR, Stork O, Pape H-C (2003) **Amygdalar and hippocampal theta rhythm synchronization during fear memory retrieval** *Science* **301**:846–850
- Song S, Miller KD, Abbott LF (2000) **Competitive Hebbian learning through spike-timing-dependent synaptic plasticity** *Nat Neurosci* **3**:919–926
- Sosulina L, Graebenitz S, Pape H-C (2010) **GABAergic Interneurons in the Mouse Lateral Amygdala: A Classification Study** *Journal of Neurophysiology* **104**:617–626
- Spampanato J, Polepalli J, Sah P (2011) **Interneurons in the basolateral amygdala** *Neuropharmacology* **60**:765–773
- Stujenske JM, Likhtik E, Topiwala MA, Gordon JA (2014) **Fear and Safety Engage Competing Patterns of Theta-Gamma Coupling in the Basolateral Amygdala** *Neuron* **83**:919–933
- Stujenske JM, P-K O’Neill, Fernandes-Henriques C, Nahmoud I, Goldberg SR, Singh A, Diaz L, Labkovich M, Hardin W, Bolkan SS, Reardon TR, Spellman TJ, Salzman CD, Gordon JA, Liston C, Likhtik E (2022) **Prelimbic cortex drives discrimination of non-aversion via amygdala somatostatin interneurons** *Neuron* **110**:2258–2267
- Szinyei C, Narayanan RT, Pape H-C (2007) **Plasticity of inhibitory synaptic network interactions in the lateral amygdala upon fear conditioning in mice: Fear-related plasticity of amygdaloid inhibition** *European Journal of Neuroscience* **25**:1205–1211
- Tanaka T, Nakamura KC (2019) **Focal inputs are a potential origin of local field potential (LFP) in the brain regions without laminar structure** *PLoS One* **14**
- Teleńczuk B, Dehghani N, Le Van Quyen M, Cash SS, Halgren E, Hatsopoulos NG, Destexhe A (2017) **Local field potentials primarily reflect inhibitory neuron activity in human and monkey cortex** *Sci Rep* **7**
- Teleńczuk M, Teleńczuk B, Destexhe A (2020) **Modelling unitary fields and the single-neuron contribution to local field potentials in the hippocampus** *J Physiol* **598**:3957–3972
- Thompson EH, Lensjø KK, Wigestrang MB, Malthé-Sørensen A, Hafting T, Fyhn M (2018) **Removal of perineuronal nets disrupts recall of a remote fear memory** *Proc Natl Acad Sci U S A* **115**:607–612

Tort ABL, Rotstein HG, Dugladze T, Gloveli T, Kopell NJ (2007) **On the formation of gamma-coherent cell assemblies by oriens lacunosum-moleculare interneurons in the hippocampus** *Proc Natl Acad Sci U S A* **104**:13490–13495

Tovote P, Fadok JP, Lüthi A (2015) **Neuronal circuits for fear and anxiety** *Nat Rev Neurosci* **16**:317–331

Tremblay R, Lee S, Rudy B (2016) **GABAergic interneurons in the neocortex: From cellular properties to circuits** *Neuron* **91**

Trouche S, Sasaki JM, Tu T, Reijmers LG (2013) **Fear Extinction Causes Target-Specific Remodeling of Perisomatic Inhibitory Synapses** *Neuron* **80**:1054–1065

Veit J, Handy G, Mossing DP, Doiron B, Adesnik H (2023) **Cortical VIP neurons locally control the gain but globally control the coherence of gamma band rhythms** *Neuron* **111**:405–417

Whittington MA, Traub RD, Kopell N, Ermentrout B, Buhl EH (2000) **Inhibition-based rhythms: experimental and mathematical observations on network dynamics** *Int J Psychophysiol* **38**:315–336

Wolff SBE, Gründemann J, Tovote P, Krabbe S, Jacobson GA, Müller C, Herry C, Ehrlich I, Friedrich RW, Letzkus JJ, Lüthi A (2014) **Amygdala interneuron subtypes control fear learning through disinhibition** *Nature* **509**:453–458

Zhou Y, Vo T, Rotstein HG, McCarthy MM, Kopell N (2018) **M-Current Expands the Range of Gamma Frequency Inputs to Which a Neuronal Target Entrain** *J Math Neurosci* **8**

## Author information

### Anna Cattani

Department of Mathematics & Statistics, Boston University, Boston, Massachusetts, United States

**For correspondence:** [acattani@bu.edu](mailto:acattani@bu.edu)

ORCID iD: [0000-0003-2317-1737](https://orcid.org/0000-0003-2317-1737)

### Don B Arnold

Department of Biology, University of Southern California, Los Angeles, California, United States

### Michelle McCarthy

Department of Mathematics & Statistics, Boston University, Boston, Massachusetts, United States

### Nancy Kopell

Department of Mathematics & Statistics, Boston University, Boston, Massachusetts, United States

ORCID iD: [0000-0002-8568-8750](https://orcid.org/0000-0002-8568-8750)

## Editors

Reviewing Editor

### Laura Colgin

University of Texas at Austin, United States of America

## Reviewer #1 (Public Review):

Plasticity in the basolateral amygdala (BLA) is thought to underlie the formation of associative memories between neutral and aversive stimuli, i.e. fear memory. Concomitantly, fear learning modifies the expression of BLA theta rhythms, which may be supported by local interneurons. Several of these interneuron subtypes, PV+, SOM+, and VIP+, have been implicated in the acquisition of fear memory. However, it was unclear how they might act synergistically to produce BLA rhythms that structure the spiking of principal neurons so as to promote plasticity. Cattani et al. explored this question using small network models of biophysically detailed interneurons and principal neurons.

Using this approach, the authors had four principal findings:

1. Intrinsic conductances in VIP+ interneurons generate a slow theta rhythm that periodically inhibits PV+ and SOM+ interneurons, while disinhibiting principal neurons.
2. A gamma rhythm arising from the interaction between PV+ and principal neurons establishes the precise timing needed for spike-timing-dependent plasticity.
3. Removal of any of the interneuron subtypes abolishes conditioning-related plasticity.
4. Learning-related changes in principal cell connectivity enhance the expression of slow theta in the local field potential.

The strength of this work is that it explores the role of multiple interneuron subtypes in the formation of associative plasticity in the basolateral amygdala. The authors use biophysically detailed cell models that capture many of their core electrophysiological features, which helps translate their results into concrete hypotheses that can be tested *in vivo*. Moreover, they try to align the connectivity and afferent drive of their model with those found experimentally. However, the weakness is that their attempt to align with the experimental literature (specifically Krabbe et al. 2019) is performed inconsistently. Some connections between cell types were excluded without adequate justification (e.g. SOM+ to PV+). In addition, the construction of the afferent drive to the network does not reflect the stimulus presentations that are given in fear conditioning tasks. For instance, the authors only used a single training trial, the conditioning stimulus was tonic instead of pulsed, the unconditioned stimulus duration was artificially extended in time, and its delivery overlapped with the neutral stimulus, instead of following its offset. These deviations undercut the applicability of their findings.

This study partly achieves its aim of understanding how networks of biophysically distinctive interneurons interact to generate nested rhythms that coordinate the spiking of principal neurons. What still remains to demonstrate is that this promotes plasticity for training protocols that emulate what is used in studies of fear conditioning.

Setting aside the issues with the conditioning protocol, the study offers a model for the generation of multiple rhythms in the BLA that is ripe for experimental testing. The most promising avenue would be *in vivo* experiments testing the role of local VIP+ neurons in the generation of slow theta. That would go a long way to resolving whether BLA theta is locally generated or inherited from medial prefrontal cortex or ventral hippocampus afferents.

The broader importance of this work is that it illustrates that we must examine the function of neurons not just in terms of their behavioral correlates, but by their effects on the microcircuit they are embedded within. No one cell type is instrumental in producing fear learning in the BLA. Each contributes to the orchestration of network activity to produce

plasticity. Moreover, this study reinforces a growing literature highlighting the crucial role of theta and gamma rhythms in BLA function.

## Reviewer #2 (Public Review):

The authors of this study have investigated how oscillations may promote fear learning using a network model. They distinguished three types of rhythmic activities and implemented an STDP rule to the network aiming to understand the mechanisms underlying fear learning in the BLA. My comments are the following.

1. Gamma oscillations are generated locally; thus, it is appropriate to model in any cortical structure. However, the generation of theta rhythms is based on the interplay of many brain areas therefore local circuits may not be sufficient to model these oscillations. Moreover, to generate the classical theta, a laminal structure arrangement is needed (where neurons form layers like in the hippocampus and cortex)(Buzsaki, 2002), which is clearly not present in the BLA. To date, I am not aware of any study which has demonstrated that theta is generated in the BLA. All studies that recorded theta in the BLA performed the recordings referenced to a ground electrode far away from the BLA, an approach that can easily pick up volume conducted theta rhythm generated e.g., in the hippocampus or other layered cortical structure. To clarify whether theta rhythm can be generated locally, one should have conducted recordings referenced to a local channel (see Lalla et al., 2017 eNeuro). In summary, at present, there is no evidence that theta can be generated locally within the BLA. Though, there can be BLA neurons, firing of which shows theta rhythmicity, e.g., driven by hippocampal afferents at theta rhythm, this does not mean that theta rhythm per se can be generated within the BLA as the structure of the BLA does not support generation of rhythmic current dipoles. This questions the rationale of using theta as a proxy for BLA network function which does not necessarily reflect the population activity of local principal neurons in contrast to that seen in the hippocampus.

2. The authors distinguished low and high theta. This may be misleading, as the low theta they refer to is basically a respiratory-driven rhythm typically present during an attentive state (Karalis and Sirota, 2022; Bagur et al., 2021, etc.). Thus, it would be more appropriate to use breathing-driven oscillations instead of low theta. Again, this rhythm is not generated by the BLA circuits, but by volume conducted into this region. Yet, the firing of BLA neurons can still be entrained by this oscillation. I think it is important to emphasize the difference.

3. The authors implemented three interneuron types in their model, ignoring a large fraction of GABAergic cells present in the BLA (Vereczki et al., 2021). Recently, the microcircuit organization of the BLA has been more thoroughly uncovered, including connectivity details for PV interneurons, firing features of neurochemically identified interneurons (instead of mRNA expression-based identification, Sosulina et al., 2010), synaptic properties between distinct interneuron types as well as principal cells and interneurons using paired recordings. These recent findings would be vital to incorporate into the model instead of using results obtained in the hippocampus and neocortex. I am not sure that a realistic model can be achieved by excluding many interneuron types.

4. The authors set the reversal potential of GABA-A receptor-mediated currents to -80 mV. What was the rationale for choosing this value? The reversal potential of IPSCs has been found to be -54 mV in fast-spiking (i.e., parvalbumin) interneurons and around -72 mV in principal cells (Martina et al., 2001, Veres et al., 2017).

5. Proposing neuropeptide VIP as a key factor for learning is interesting. Though, it is not clear why this peptide is more important in fear learning in comparison to SST and CCK, which are also abundant in the BLA and can effectively regulate the circuit operation in cortical areas.

## Reviewer #3 (Public Review):

### Summary:

The authors present a biophysically detailed model of the basolateral amygdala (BLA) that is capable of fear learning through a depression-dominated spike-timing dependent plasticity (STDP) mechanism. Furthermore, the model also replicates experimentally measured rhythmic signatures of baseline amygdala activity and changes of these signatures during and after fear learning. The authors furthermore carefully dissect the contributions of the three different types of interneurons (parvalbumin-positive (PV), somatostatin-positive (SOM), and vaso-active peptide-positive (VIP) interneurons) in regulating network activity to allow for the association between conditioned and unconditioned stimuli.

### Strengths:

The biophysical detail of the model allows the authors to go beyond a simple modelling of the fear learning process in terms of spiking activity of the principal cells and to link the associative learning to several oscillatory rhythms in the BLA, namely high and low theta and gamma rhythms. This provides an understanding of the generation and function of these rhythms in the baseline amygdala circuit as well as of the functional consequences of alterations of these rhythms during and after the fear learning process. This offers a new and uniquely detailed insight into the mechanistic level.

### Weaknesses:

The main weakness of the approach is the lack of experimental data from the BLA to constrain the biophysical models. This forces the authors to use models based on other brain regions and leaves open the question of whether the model really faithfully represents the basolateral amygdala circuitry. Furthermore, the authors chose to use model neurons without a representation of the morphology. However, given that PV and SOM cells are known to preferentially target different parts of pyramidal cells and given that the model relies on a strong inhibition from SOM to silence pyramidal cells, the question arises whether SOM inhibition at the apical dendrite in a model representing pyramidal cell morphology would still be sufficient to provide enough inhibition to silence pyramidal firing. Lastly, the fear learning relies on the presentation of the unconditioned stimulus over a long period of time (40 seconds). The authors justify this long-lasting input as reflecting not only the stimulus itself but as a memory of the US that is present over this extended time period. However, the experimental evidence for this presented in the paper is only very weak.

The authors achieved the aim of constructing a biophysically detailed model of the BLA not only capable of fear learning but also showing spectral signatures seen *in vivo*. The presented results support the conclusions with the exception of a potential alternative circuit mechanism demonstrating fear learning based on a classical Hebbian (i.e. non-depression-dominated) plasticity rule, which would not require the intricate interplay between the inhibitory interneurons. This alternative circuit is mentioned but a more detailed comparison between it and the proposed circuitry is warranted.

The presented model demonstrates how the complex interplay between different types of interneurons is able to precisely control neural activity to enable learning to happen. Furthermore, the presented work shows this interactive control of activity by the interneurons gives rise to specific oscillatory signatures. Since the three types of interneurons considered here are found throughout the brain, the findings will likely have a big impact on other studies of interneuron function and learning in general.

## Author Response

We thank the reviewers for their work and their thoughtfulness. However, it seems to us that much (but not all) of the critique reflects a misunderstanding of the goals and methods of computational modeling. Details are below. We are grateful for the opportunity to include our views about this in the context of our replies to the Public Critiques of our paper. The comments of the reviewers were very helpful in allowing us to see what might not be clear to our readers.

### ***eLife assessment***

*This useful modeling study explores how the biophysical properties of interneuron subtypes in the basolateral amygdala enable them to produce nested oscillations whose interactions facilitate functions such as spike-timing-dependent plasticity. The strength of evidence is currently viewed as incomplete because the relevance to plasticity induced by fear conditioning is viewed as insufficiently grounded in existing training protocols and prior experimental results, and alternative explanations are not sufficiently considered. This work will be of interest to investigators studying circuit mechanisms of fear conditioning as well as rhythms in the basolateral amygdala.*

Most of our comments below are intended to rebut the sentence: “The strength of evidence is currently viewed as incomplete because the relevance to plasticity induced by fear conditioning is viewed as insufficiently grounded in existing training protocols and prior experimental results, and alternative explanations are not sufficiently considered”. Details are below in the answer to reviewers.

We believe this work will be interesting to investigators interested in dynamics associated with plasticity, which goes beyond fear learning. It will also be of interest because of its emphasis on the interactions of multiple kinds of interneurons that produce dynamics used in plasticity, in the cortex (which has similar interneurons) as well as BLA.

We note that the model has sufficiently detailed physiology to make many predictions that can be tested experimentally. In the revision, we will be more explicit about this.

We thank Reviewer #1 for stressing our work's important contribution to providing concrete hypotheses that can be tested in vivo and highlighting the importance of examining in the future the synergistic role of the interneurons in the BLA in fear learning in the BLA. The weaknesses reported by the Reviewer concern deviations of the model compared to the experimental literature. We describe below why we think those differences are minor in the context of the aims of our model. Specifically,

1. *Some connections among neurons in the BLA reported by (Krabbe et al., 2019) have not been taken into account in the model. Some connections between cell types were excluded without adequate justification (e.g. SOM+ to PV+).*

In order to constrain our model, we focused on what is reported in (Krabbe et al., 2019) in terms of functional connectivity instead of structural connectivity. Thus, we included only those connections for which there was strong functional connectivity. For example, the SOM+ to PV+ connection is shown to be small (Supp. Fig. 4, panel t). We also omitted PV+ to SOM+, PV+ to VIP+, SOM+ to VIP+, VIP+ to excitatory projection neurons; all of these are shown in (Krabbe et al. 2019, Fig. 3 (panel l), and Supp. Fig. 4 (panels m,t)) to have weak functional connectivity, at least in the context of fear conditioning. See below for comments on modeling strategies. We will explain this better in our revision.

1. *The construction of the afferent drive to the network does not reflect the stimulus presentations that are given in fear conditioning tasks. For instance, the authors only used a single training trial, the conditioning stimulus was tonic instead of pulsed, the unconditioned stimulus duration was artificially extended in time, and its delivery overlapped with the neutral stimulus, instead of following its offset. These deviations undercut the applicability of their findings.*

Regarding the use of a single long presentation of US rather than multiple presentations (i.e., multiple trials): in early versions of this paper, we did indeed use multiple presentations. We were told by experimental colleagues that the learning could be achieved in a single trial. We note that, if there are multiple presentations in our modeling, nothing changes; once the association between CS and US is learned, the conductance of the synapse is stable. Also, our model does not need a long period of US if there are multiple presentations. This point will be made clearer in our revision.

We agree that, in order to implement the fear conditioning paradigm in our in-silico network, we made several assumptions about the nature of the CS and US inputs affecting the neurons in the BLA and the duration of these inputs. A Poisson spike train to the BLA is a signal that contains no structure that could influence the timing of the BLA output; hence, we used this as our CS input signal. We also note that the CS input can be of many forms in general fear conditioning (e.g., tone, light, odor), and we wished to de-emphasize the specific nature of the CS. The reference mentioned in the Recommendations for authors, (Quirk, Armony, and LeDoux 1997), uses pulses 2 seconds long. At the end of fear conditioning, the response to those pulses is brief. However, in the early stages of conditioning, the response goes on for as long as the figure shows. The authors do show the number of cells responding decreases from early to late training, which perhaps reflects increasing specificity over training. This feature is not currently in our model, but we look forward to thinking about how it might be incorporated. Regarding the CS pulsed protocol used in (Krabbe et al., 2019), it has been shown that intense inputs (6kHz and 12 kHz inputs) can lead to metabotropic effects that last much longer than the actual input (200 ms duration) (Whittington et al., Nature, 1995). Thus, the effective input to the BLA may indeed be more like Poisson.

Our model requires the effect of the CS and US inputs on the BLA neuron activity to overlap in time in order to instantiate fear learning. Despite paradigms involving both overlapping (delay conditioning, where US coterminates with CS (Lindquist et al., 2004), or immediately follows CS (e.g., Krabbe et al., 2019)) and non-overlapping (trace conditioning) CS/US inputs existing in the literature, we hypothesized that concomitant activity in CS- and US-encoding neuron activity should be crucial in both cases. This may be mediated by the memory effect, as suggested in the Discussion of our paper, or by metabotropic effects as suggested above, or by the contribution from other brain regions. We will emphasize in our revision that the overlap in time, however instantiated, is a hypothesis of our model. It is hard to see how plasticity can occur without some memory trace of US. This is a consequence of our larger hypothesis that fear learning uses spike-timing-dependent plasticity; such a hypothesis about plasticity is common in the modeling literature. We will discuss these points in more detail in our revision.

We thank Reviewer #2 for their comments. Below, we reply to each of them:

1. *Gamma oscillations are generated locally; thus, it is appropriate to model in any cortical structure. However, the generation of theta rhythms is based on the interplay of many brain areas therefore local circuits may not be sufficient to model these oscillations. Moreover, to generate the classical theta, a laminal structure arrangement is needed (where neurons form layers like in the hippocampus and cortex)(Buzsaki, 2002), which is clearly not present in the BLA. To date, I am not aware of any study which has*

*demonstrated that theta is generated in the BLA. All studies that recorded theta in the BLA performed the recordings referenced to a ground electrode far away from the BLA, an approach that can easily pick up volume conducted theta rhythm generated e.g., in the hippocampus or other layered cortical structure. To clarify whether theta rhythm can be generated locally, one should have conducted recordings referenced to a local channel (see Lalla et al., 2017 eNeuro). In summary, at present, there is no evidence that theta can be generated locally within the BLA. Though, there can be BLA neurons, firing of which shows theta rhythmicity, e.g., driven by hippocampal afferents at theta rhythm, this does not mean that theta rhythm per se can be generated within the BLA as the structure of the BLA does not support generation of rhythmic current dipoles. This questions the rationale of using theta as a proxy for BLA network function which does not necessarily reflect the population activity of local principal neurons in contrast to that seen in the hippocampus.*

In both modeling and experiments, a laminar structure does not seem to be needed to produce a theta rhythm. A recent experimental paper, (Antonoudiou et al. 2021), suggests that the BLA can intrinsically generate theta oscillations (3-12 Hz) detectable by LFP recordings under certain conditions, such as reduced inhibitory tone. The authors draw this conclusion by looking at mice *ex vivo* slices. The currents that generate these rhythms are in the BLA, since the hippocampus was removed to eliminate hippocampal volume conduction and other nearby brain structures did not display any oscillatory activity. Also, in the modeling literature, there are multiple examples of the production of theta rhythms in small networks not involving layers; these papers explain the mechanisms producing theta from non-laminated structures (Dudman et al., 2009, Kispersky et al., 2010, Chartove et al. 2020). We are not aware of any model description of the mechanisms of theta that do require layers.

*1. The authors distinguished low and high theta. This may be misleading, as the low theta they refer to is basically a respiratory-driven rhythm typically present during an attentive state (Karalis and Sirota, 2022; Bagur et al., 2021, etc.). Thus, it would be more appropriate to use breathing-driven oscillations instead of low theta. Again, this rhythm is not generated by the BLA circuits, but by volume conducted into this region. Yet, the firing of BLA neurons can still be entrained by this oscillation. I think it is important to emphasize the difference.*

Many rhythms of the nervous system can be generated in multiple parts of the brain by multiple mechanisms. We do not dispute that low theta appears in the context of respiration; however, this does not mean that other rhythms with the same frequencies are driven by respiration. Indeed, in the above answer we showed that theta can appear in the BLA without inputs from other regions. In our paper, the low theta is generated in the BLA by VIP+ neurons. Using intrinsic currents known to exist in VIP+ neurons (Porter et al., 1998), modeling has shown that such neurons can intrinsically produce a low theta rhythm. This is also shown in the current paper. This example is part of a substantial literature showing that there are multiple mechanisms for any given frequency band. We will emphasize these points in our revision; we note that, for any individual case, such as this one, the mechanism needs to be tested experimentally.

*1. The authors implemented three interneuron types in their model, ignoring a large fraction of GABAergic cells present in the BLA (Vereczki et al., 2021). Recently, the microcircuit organization of the BLA has been more thoroughly uncovered, including connectivity details for PV+ interneurons, firing features of neurochemically identified interneurons (instead of mRNA expression-based identification, Sosulina et al., 2010), synaptic properties between distinct interneuron types as well as principal cells and interneurons using paired recordings. These recent findings would be vital to incorporate*

*into the model instead of using results obtained in the hippocampus and neocortex. I am not sure that a realistic model can be achieved by excluding many interneuron types.*

The interneurons and connectivity that we used were inspired by the functional connectivity reported in (Krabbe et al., 2019) (see above answer to Reviewer #1). As reported in (Vereczki et al., 2021), there are multiple categories and subcategories of interneurons; that paper does not report on which ones are essential for fear conditioning. We did use all the highly represented categories of the interneurons, except NPY-containing neurogliaform cells.

The Reviewer says “I am not sure that a realistic model can be achieved by excluding many interneuron types”. We agree with the Reviewer that discarding the introduction of other interneurons subtypes and the description of more specific connectivity (soma-, dendrite-, and axon-targeting connections) may limit the ability of our model to describe all the details in the BLA. However, this work represents a first effort towards a biophysically detailed description of the BLA rhythms and their function. As in any modeling approach, assumptions about what to describe and test are determined by the scientific question; details postulated to be less relevant are omitted to obtain clarity. The interneuron subtypes we modeled, especially VIP+ and PV+, have been reported to have a crucial role in fear conditioning (Krabbe et al., 2019). Other interneurons, e.g. cholecystokinin and SOM+, have been suggested as essential in fear extinction. Thus, in the follow-up of this work to explain fear extinction, we will introduce other cell types and connectivity. In the current work, we have achieved our goals of explaining the origin of the experimentally found rhythms and their roles in the production of plasticity underlying fear learning. Of course, a more detailed model may reveal flaws in this explanation, but this is science that has not been yet done.

*1. The authors set the reversal potential of GABA-A receptor-mediated currents to -80 mV. What was the rationale for choosing this value? The reversal potential of IPSCs has been found to be -54 mV in fast-spiking (i.e., parvalbumin) interneurons and around -72 mV in principal cells (Martina et al., 2001, Veres et al., 2017).*

A GABA-A reversal potential around -80 mV is common in the modeling literature (Jensen et al., 2005; Traub et al., 2005; Kumar et al., 2011; Chartove et al., 2020). Other computational works of the amygdala, e.g. (Kim et al., 2016), consider GABA-A reversal potential at -75 mV based on the cortex (Durstewitz et al., 2000). The papers cited by the reviewer have a GABA-A reversal potential of -72 mV for synapses onto pyramidal cells; this is sufficiently close to our model that it is not likely to make a difference. For synapses onto PV+ cells, the papers cited by the reviewer suggest that the GABA-A reversal potential is -54 mV; such a reversal potential would lead these synapses to be excitatory instead of inhibitory. However, it is known (Krabbe et al., 2019; Supp. Fig. 4b) that such synapses are in fact inhibitory. Thus, we wonder if the measurements of Martina and Veres were made in a condition very different from that of Krabbe. For all these reasons, we consider a GABA-A reversal potential around -80 mV in amygdala to be a reasonable assumption. We will discuss these points in our revision.

*1. Proposing neuropeptide VIP as a key factor for learning is interesting. Though, it is not clear why this peptide is more important in fear learning in comparison to SST and CCK, which are also abundant in the BLA and can effectively regulate the circuit operation in cortical areas.*

We do not think that VIP is necessarily more fundamental in fear learning, and certainly not for fear extinction. We will make this clear in the revision.

We thank Reviewer #3 for their comments and for recognizing that we achieved our modeling aims. We reply to the criticisms below.

#### Weaknesses:

*The main weakness of the approach is the lack of experimental data from the BLA to constrain the biophysical models. This forces the authors to use models based on other brain regions and leaves open the question of whether the model really faithfully represents the basolateral amygdala circuitry. Furthermore, the authors chose to use model neurons without a representation of the morphology. However, given that PV+ and SOM+ cells are known to preferentially target different parts of pyramidal cells and given that the model relies on a strong inhibition from SOM to silence pyramidal cells, the question arises whether SOM inhibition at the apical dendrite in a model representing pyramidal cell morphology would still be sufficient to provide enough inhibition to silence pyramidal firing. Lastly, the fear learning relies on the presentation of the unconditioned stimulus over a long period of time (40 seconds). The authors justify this long-lasting input as reflecting not only the stimulus itself but as a memory of the US that is present over this extended time period. However, the experimental evidence for this presented in the paper is only very weak.*

Many of these issues were addressed in the previous responses.

1. Our neurons were constrained by electrophysiology properties in response to hyperpolarizing currents in the BLA (Sosulina et al., 2010). We choose the specific currents, known to be present in these neurons, to replicate those responses.
2. Though a much more detailed description of BLA interneurons was given in (Vereczki et al., 2021), it is not clear that this level of detail is relevant to the questions that we were asking, especially since the experiments described were not done in the context of fear learning.
3. It is true that we did not include the morphology, which undoubtedly makes a difference to some aspects of the circuit dynamics. As we described above, modeling requires the omission of many details to bring out the significance of other details.
4. As described above, some form of memory or overlap in the activity of the excitatory projection neurons is necessary for spike-timing-dependent plasticity. In modeling, one must be specific about hypotheses, and describe why they are plausible, if not proved; indeed, modeling can explain known phenomena by showing how they are consequences of some (plausible) hypotheses, which themselves are open to experimental verification.
5. The 40 seconds is not necessary if there are multiple presentations.

#### Other critiques:

1. It is correct that PV+ and SOM+ preferentially target different parts of excitatory projection neurons and that the model relies on a strong inhibition from SOM+ and PV+ to silence the excitatory projection neurons. This choice of parameters comes from using simplified models: it is standard in modeling to adjust parameters to compensate for simplifications.
2. The SOM+ inhibition of the pyramidal cell firing can be seen as a hypothesis of our model. It is well known that VIP+ cells disinhibit pyramidal cells through inhibition of SOM+ and PV+ cells, which is all we are using in our model; hence this hypothesis is generally believed.

*The authors achieved the aim of constructing a biophysically detailed model of the BLA not only capable of fear learning but also showing spectral signatures seen in vivo. The*

*presented results support the conclusions with the exception of a potential alternative circuit mechanism demonstrating fear learning based on a classical Hebbian (i.e. non-depression-dominated) plasticity rule, which would not require the intricate interplay between the inhibitory interneurons. This alternative circuit is mentioned but a more detailed comparison between it and the proposed circuitry is warranted.*

We agree with the reviewer that it would be good to have a more detailed comparison with the classical Hebbian rule (non-depression-dominated rule). However, we demonstrated in Supplementary Materials that the non-depression-dominated rule is less robust and only operates within a limited window of PV+ excitation. We will have a more robust discussion of plasticity in the revision.